Nanoscale

Accepted Manuscript

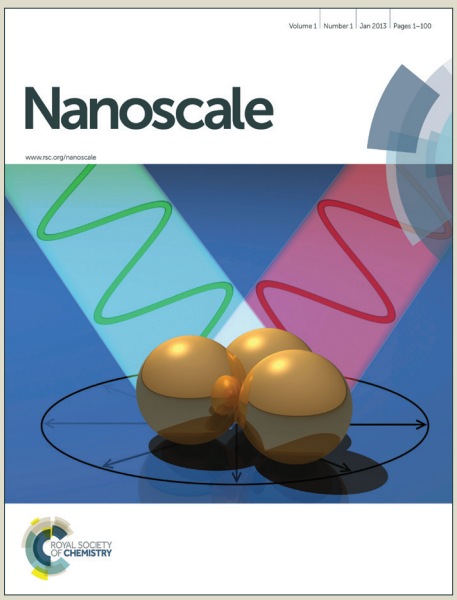

ROYAL SOCIETY OF CHEMISTRY

www.rsc.org/nanoscale

Recent Progress in Magnetic Iron Oxide-Semiconductor Composite Nanomaterials as Promising Photocatalysts

Wei Wu[1, 2]*, *Changzhong Jiang*[3] *and Vellaisamy A.L. Roy*[2]*

[1] Laboratory of Printable Functional Nanomaterials and Printed Electronics, School of Printing and Packaging, Wuhan University, Wuhan 430072, P. R. China

[2] Department of Physics and Materials Science, City University of Hong Kong, Hong Kong SAR, P. R. China

[3] Key Laboratory of Artificial Micro- and Nano-structures of Ministry of Education, School of Physics and Technology, Wuhan University, Wuhan 430072, P. R. China

Corresponding author: weiwu@whu.edu.cn (W. Wu) and val.roy@cityu.edu.hk (V. A. L. Roy)

Abstract

Photocatalytic degradation of toxic organic pollutants is one of the challenging tasks in ecological and environmental protection. Recent researches show that the magnetic iron oxide semiconductor composite photocatalytic system can effectively break through the bottleneck of single-component semiconductor oxides that have low activity under visible light and challenging to recycle from the products. With high reactivity in the visible light, magnetic iron oxide semiconductors can be exploited as an important magnetic recovery photocatalyst (MRPs) with a bright future. On this regard, the types of various composite structure, charge-transfer mechanism and outstanding properties of magnetic iron oxide semiconductor composite nanomaterials are sketched. The latest synthesis methods and recent progresses in the photocatalytic applications of magnetic iron oxide semiconductor composite nanomaterials are reviewed. The problems and challenges that still need to be resolved are pointed out and the development strategies are discussed.

Keywords: Magnetic iron oxide; Semiconductors; Photocatalyst; Heterostructures; Composite nanomaterials

1. Introduction

Our surrounding environment becomes more polluted, and the traditional chemical methods to deal with environmental pollution have been unable to meet the requirements of modern energy-saving theme and environmental protection. Environmental problems induced by toxic and hardly-degradable organic pollutants (such as halides, dioxins, pesticides, dyes, *etc.*) have posed a grave menace to human well-being and development in 21st century. Photocatalysis refers to the rate of photoreactions (oxidation/reduction) brought by the activation of a catalyst, usually a semiconductor oxide and illuminated under the ultraviolet (UV) or visible light. Use of semiconductor oxide nanomaterials-based photocatalysts to degrade organic pollutants is recognized as one of the most promising areas of research and application.[1-3] On this regard, photocatalysts are used into the solid-liquid reaction system, especially for the treatment of toxic waste.

However, the main restriction factor of large scale practical applications of semiconductor oxide photocatalyst are follows: (1) High recombination rate of electronic-hole pairs resulting in low quantum yield for single-component semiconductor oxide photocatalyst. For instance, Sun and Bolton have reported less than 5% primary quantum yield of •OH radical generation in TiO_2 suspension.[4] (2) The limitation in the harvest of visible light. Generally, wide bandgap semiconductor oxides are employed as photocatalysts, for example, the bandgap value of anatase TiO_2 is 3.2 eV, and the corresponding absorption wavelength is 387.5 nm, resulting in limited light absorption of UV. Unfortunately solar spectrum consists only 5-7% of UV light, while 46% and 47% of the spectrum has visible light and infrared radiation, respectively.[5] (3) Poor selective adsorption

and the complexity of intermediate products. For example, photodegradation reaction products such as CO_2 and H_2O are easily adsorbed on the surface of TiO_2 in the gas-solid photocatalyst system due to its super-hydrophilicity and active sites.[6] The high oxidization potential energy of OH radicals can induce many backward reactions, such as oxidizing the intermediates and products converted from the as-adsorbed CO_2.[7, 8] (4) The photocatalytic treatment of high concentration organic pollutants from industrial waste poisons the photocatalyst resulting deactivation. In addition, it is difficult to separate a pure semiconductor oxide photocatalyst from the waste water treating system,[9] which further deactivates the photocatalysts. (5) High cost of photocatalyst industrialization. This factor limits the industrial applications of photocatalyst, hence research and development of low-cost, high-performance, and recyclable photocatalyst have became an important issue.[10, 11]

As a hot issue, photocatalysis has witnessed a sea of change over the past two decades with significant advancements being made in the preparing of novel materials and nanostructures, and the design of efficient processes for the photodegradation of pollutants and the generation of energy. Thus, the development of a simple recyclable photocatalyst can not only prevent excessive use of photocatalysts, but also the recovery of deactivated photocatalysts, thereby reducing the total cost, and further lower the overall usage of the photocatalytic material. Since visible light constitutes a large fraction of solar energy, one of the great challenges for photocatalyst study is to devise new catalysts that exhibit high activity under illumination by visible light.

Combining the magnetic iron oxide nanomaterials with semiconductor nanomaterials to form magnetic iron oxide/semiconductor composite photocatalyst system become a simple and effective method. In iron oxide/semiconductor system, iron oxide has many advantages, for example, low cost, high stability and compatibility, it not only plays the role of separating the photocatalyst from the

solution, but also it can degrade the organic pollutants.[12, 13] The common metal oxide semiconductors like titanium dioxide (TiO_2), zinc oxide (ZnO), tungsten oxide (WO_3), tin oxide (SnO_2) are proven to be dynamic photocatalysts for organic dyes and pollutants, these semiconductors not only destroy the conjugated chromophoric system, but also breakdown the molecular structure of the organic dyes and pollutants into harmless CO_2 and H_2O. As magnetic recovery photocatalytic materials, iron oxide/semiconductor oxides photocatalyst system can be effectively break through the bottleneck of lower activity under visible light and demanding recycling process from the products, and eventually become a potential visible light responsive MRPs in future.

Therefore, the design of iron oxide-semiconductor photocatalytic system is an essential prerequisite for both basic and applied research. If the system focuses on the magnetic recovery properties, the saturation magnetization value of used iron oxides should be not less than 1 emu/g, in order to separate by external magnetic field for further reusing and regeneration. If the system focuses on the photocatalytic performance, the used iron oxides should possess a relatively narrow bandgap value. For instance, goethite and hematite are often studied as photocatalysts in recent years because of their low band gap (2.2 eV). There are reported techniques to improve the photocatalytic performance of iron oxide-semiconductor system, such as composite heterostructure with narrow/wide bandgap, p-n heterojunctions, noble metal loading, plasmonic structure, graphene loading, etc.[14-16] Overall, an optimal iron oxide-semiconductor photocatalytic system design should meet the following requirements. First, the synthesis and preparation process should be both simple, facile with high-yield. Second, the composite system should exhibit an enhanced photocatalytic performance remarkably superior to existing naked iron oxide and pure semiconductor materials. Third, the composite photocatalyst should be recycled by the external

magnetic field that facilitates easy reuse and regeneration. Finally, the composite photocatalyst should possess good photocorrosion resistance ability and stable at room temperature for months.

In this review, we will first describe the structure and mechanism of magnetic iron oxide-semiconductor photocatalysis system. We discuss different synthesis methods and recent advances of magnetic iron oxide-semiconductor nanomaterials. The potential of magnetic iron oxide-semiconductor based materials as photocatalysts is also examined. Finally, we discuss future prospects in realizing this technology and research directions.

2 Structure and mechanism for magnetic iron oxide-semiconductor composite photocatalysts

2.1 Magnetic iron oxides nanomaterials

As a common compound, iron oxide is widely distributed in nature and could be synthesized in large-scale. The application of small iron oxide nanoparticles has been practiced in *in vitro* diagnostics for more than 60 years.[17] Over the past few decades, the magnetic iron oxide nanoparticles with various morphologies and structures are widely fabricated because of the importance of basic research. On the other hand, magnetic iron oxides are of great interest for researchers due to wide range of applications, including pigments, magnetic fluids, catalysis, targeted drug delivery, biosensor, magnetic resonance imaging, data storage, and environmental remediation.[13, 18, 19] The iron oxides are composed of Fe together with O. There are eight iron oxides known to data.[20] Among iron oxides, the hematite (α-Fe_2O_3), magnetite (Fe_3O_4) and maghemite (γ-Fe_2O_3) are the promising and popular candidates due to their polymorphism involving temperature induced phase transition. These three different crystalline iron oxides have unique biochemical, magnetic, catalytic, and other properties that make them suitable for specific technical and biomedical applications.

Magnetic measurements of the α-Fe_2O_3 show obvious weak ferromagnetism, and its saturation magnetization is often less than 1 emu/g at room temperature. However, the γ-Fe_2O_3 and Fe_3O_4 show saturation magnetization up to 92 emu/g.[21] More importantly, the magnetic properties of iron oxide nanoparticles are related to its size and shape. For example, Demortière and co-workers have investigated the size-dependence of iron oxide nanocrystals on their structural and magnetic properties by fine tuning the size within the nanometer scale (diameters range from 2.5 to 14 nm). The evolution of the magnetic behavior with nanoparticle size emphasizes clearly the influence of the surface, especially on the saturation magnetization (M_s) and the magneto-crystalline anisotropy. Dipole interactions and thermal dependence have also been taken into account on the study of nanoscale size-effect on magnetic properties.[22] More recently, we have reported a comparative study on the magnetic behavior of single and tubular clustered Fe_3O_4 nanoparticles. The results reveal that the coercivity of small iron oxide nanoparticles could be enhanced by the competition between the demagnetization energy of morphology and magnetocrystalline anisotropy energy.[23] Choi and co-workers have prepared Fe_3O_4 nanoparticles with different shapes, including solid nanospheres and solid/hollow nanoellipsoids. All these structures were obtained by either adding the appropriate amount of sodium acetate (NaOAc) or using the anion exchange of β-FeOOH. All magnetite nanoparticles exhibited ferromagnetic behaviour with different values of saturation magnetization (M_s) and coercivity (H_c), and these values are highly depend on the shape due to their grain size, spin disorder, shape, and surface anisotropy.[24] In general, iron oxide nanoparticles become superparamagnetic at room temperature when the size of iron oxide nanoparticles are below ca. 15 nm, meaning that the thermal energy can overcome the anisotropy energy barrier of a single nanoparticle. If the semiconductor is coated on the surface of iron oxide, the M_s value would decrease. There are number of magnetic properties for the characterization of naked iron oxides

nanoparticles and iron oxides-semiconductor composite nanomaterials. The most important properties are the type and magnetization and can be determined from the hysteresis loops (M-H) and zero-field cooled/ field cooled (ZFC/FC, M-T) curves. As shown in **Figure 1**, the saturation magnetization (M_S), remanence magnetization (M_r), corecivity (H_C) can be obtained from the hysteresis loop. When the naked iron oxide nanoparticles and iron oxide-semiconductor composite nanomaterials exhibit superparamagnetic, the M-H curve should show no hysteresis at a certain temperature ($T > T_B$, blocking temperature). The forward and backward magnetization curves overlap completely.[23, 25]

The general strategy for preparing magnetic iron oxide nanoparticles in solution phase is to separate the nucleation and growth of nanocrystals. Numerous synthetic methods have been developed to synthesize magnetic iron oxide NPs, including co-precipitation,[26-28] high-temperature thermal decomposition,[29-31] hydrothermal and solvothermal reaction,[32-34] sol-gel reactions and polyol method,[25, 35, 36] microemulsion synthesis,[37-39] sonochemical reaction,[40-44] microwave-assisted synthesis[45-48] and biosynthesis.[49-51] Except the above-mentioned methods, other chemical or physical methods can also be used to synthesize magnetic iron oxide nanoparticles, such as the electrochemical methods,[52-54] flow injection synthesis,[55] aerosol/vapor methods,[56-58] etc. In literature, there are reports on the fabrication of magnetic iron oxide NPs. Here, we briefly review the recent advances on the synthesis of magnetic iron oxide-semiconductor composite nanomaterials (in Section 3).

2.2 Semiconductor nanomaterials

Semiconductor oxides (e.g., TiO_2, ZrO_2, ZnO, WO_3, MoO_3, SnO_2, α-Fe_2O_3, *etc.*) and semiconductor sulfides (e.g., ZnS, CdS, CdSe, WS_2, MoS_2, *etc.*) can use as catalysts for

photoinduced chemical reactions due to their intrinsic electronic structure that consist of a filled valence band (VB) and an empty conduction band (CB).[59-64] When a photon with energy ($h\nu$) matches or exceeds the band gap energy (E_g) of the semiconductor, a photogenerated electron (e^-) in the valence band is excited into the conduction band, leaving a positive hole (h^+) in the valence band. The photoinduced charge carriers play a key role in photocatalytic degradation process. The holes mediate the oxidation of organic compounds by the formation of hydroxyl radicals (•OH), and the electrons mediate redox reactions by the formation of superoxide radicals ($\bullet O_2$). However, the photoinduced charge carriers in the excited states are unstable and can easily recombine, converting the input energy to heat and thus leading to the low activity of photocatalyst.[65] An ideal photocatalyst should be stable, inexpensive, non-toxic and, of course, highly photoactive.

On the basis of thermodynamic requirements, the VB and CB of the semiconductor photocatalyst should be located in such a way that, the oxidation potential of the hydroxyl radicals ($E_0(H_2O/\bullet OH)$ = 2.8 V vs NHE) and the reduction potential of superoxide radicals ($E_0(O_2/\bullet O_2^-)$ = −0.28 V vs NHE), lie well within the band gap. In other words, the redox potential of VB holes must be enough positive to produce hydroxyl radicals. On the other hand, the CB electrons must be enough negative to produce superoxide radicals.[66] **Figure 2** shows the bandgap energy and band edge positions of common semiconductor oxides and semiconductor sulfides, along with selected redox potentials. Obviously, the bandgap energy and band edge positions of TiO_2, ZnO, SnO_2, Fe_2O_3, WO_3 and ZrO_2 are relatively good. As already mentioned, such semiconductors materials are prone to apply in photocatalysis due to its inherent filled VB and empty CB. When these semiconducting solids absorb photons and $h\nu \geq E_g$, it excites an e^- from the VB to the CB. This can be expressed a formula as follows: $h\nu$ + semiconductor → $h^+ + e^-$. Then the electron of semiconductor could transfer to an adjacent compound.

Additionally, the choice of semiconductor materials for photocatalytic application rely on the consideration of photocorrosion resistance ability. For instance, CdS and ZnO have only a stable valence of +2, and can be decomposed by photogenerated holes from VB. Furthermore, ZnO is prone to be deactivated due to the generation of $Zn(OH)_2$ on its surface.[10] Currently, there are many methods to inhibit or delay the deactivation caused by photocorrosion, and the common method is to combine with other materials and to form composite nanomaterials.[67, 68] As compared to other materials, the oxidation state of Ti in TiO_2 can be reversibly changed (from +4 and +3), thereby TiO_2 is more stable and suitable for the photocatalytic application. Additionally, the anatase phase TiO_2 (E_g =3.2 eV) is more active for photocatalysis applications, even though rutile phase TiO_2 (E_g = 3.0 eV) possesses smaller band gap, revealing the possibility of absorption of long wavelength radiation. The CB of anatase TiO_2 is more negative compared to rutile.

In addition to the aforementioned factors, other requirements such as low-cost, non-toxic nature (environmentally benign) and easily preparing should also be taken into consideration for photocatalytic degradation reactions.

2.3 The structure of iron oxides-semiconductors composite nanomaterials

In order to increase the range of applications of iron oxide nanoparticles, some functional materials have been introduced and formed as newly composite nanostructures. Comparing with single-component nanomaterials, multiple-component nanomaterials have become the subject of extensive research due to the synergistic interaction effects between each component, which could improve the final catalytic performance. Currently, wide band gap semiconductors with good photocatalytic properties have been used to functionalize the magnetic iron oxides. In iron oxide-semiconductor composite system, the magnetic iron oxide not only can separate and recover the photocatalyst, but also able to form narrow/wide band gap semiconductor heterostructures. The

narrow/wide band gap semiconductor heterostructures can promote the separation of electron and hole pairs efficiently. Consequently increasing the visible light utilization and finally improve the photocatalytic efficiency.

As shown in **Figure 3**, if the iron oxide nanoparticles are always assumed to be as core, the structure of iron oxide-semiconductor composite nanomaterials can be simply divided into four types: core-shell structure, matrix-dispersed structure, Janus structure and shell-core-shell structure.

Core-shell Structure. In this structure, the iron oxides core is encapsulated by a semiconductor layer that renders the stability of the whole particle. Generally, the iron oxide nanoparticles are not located at the centre of functional semiconductor and this is known as yolk structure. For example, Liu and co-workers have successfully synthesized various Fe_3O_4@TiO_2 yolk-shell microspheres with different core sizes, interstitial void volumes, and shell thicknesses by controlling the synthetic parameters.[69] Li and core-workers have developed a facile "hydrothermal etching assisted crystallization" method to prepare Fe_3O_4@TiO_2 yolk-shell microspheres with ultrathin nanosheets assembled as double-shell structure. The as-obtained microspheres possess high surface area, good structural stability and large magnetization, the size is uniform and the shell could tailor, which exhibits versatile ion-exchange capability and a remarkable catalytic performance.[70] Indeed, the magnetic composite nanomaterials not only provide the material with an improved stability of the nanoparticulate building blocks, but also introduce new physical and chemical properties and multifunctional behaviours. In the inverse core-shell structure, the magnetic iron oxides are coated on the surface of semiconductor materials. For instance, Luo and co-workers have fabricated highly ordered TiO_2@α-Fe_2O_3 core/shell arrays on carbon textiles by a stepwise, seed-assisted, hydrothermal approach. The fabrication strategy is facile, cost-effective, and scalable, which opens new avenues for the design of optimal composite electrode materials.[71] Moreover, magnetic iron

oxides could be combined and coated with one or more functional materials on the surface of another functional material. The above structures are all called as core-shell structure.

Matrix-dispersed Structure. Several magnetic iron oxide nanoparticles are coated or dispersed in a semiconductor matrix. Matrix-dispersed nanoparticles can be created in a variety of different photocatalytic reaction states. For example, Wang and co-workers have prepared $(\gamma\text{-}Fe_2O_3@SiO_2)_n@TiO_2$ functional hybrid nanoparticles by an easy chemical route. Several $\gamma\text{-}Fe_2O_3$ fine particles about 15 nm in diameter as cores distributed in the TiO_2 matrix with silica as barrier layer between the magnetic cores and TiO_2 shells has been reported. The hybrid nanoparticles show good magnetic response and display high photocatalytic efficiency for methylene blue (MB).[72]

Janus Structure. In Janus structure, one side is magnetic iron oxide nanoparticles, and the other side is a functional semiconductor material. Anisotropic surface chemical makeup is interesting for applications even without self-assembly. For example, Zeng and co-workers have synthesized multifunctional Fe_3O_4-TiO_2 nanocomposites with Janus structure for magnetic resonance imaging (MRI) and potential photodynamic therapy (PDT), in which Fe_3O_4 is a MRI contrast agent and TiO_2 is an inorganic photosensitizer for PDT.[73] Mou and co-workers have developed an asymmetric shrinkage approach for the fabrication of magnetic $\gamma\text{-}Fe_2O_3/TiO_2$ Janus hollow bowls by constructing a precursor solution pair with different gelation rates during the solvents evaporation process. The as-obtained products exhibited an efficient visible-light photocatalytic activity and convenient magnetic separation because of the unique structure and morphology as well as the fine magnetic properties.[74]

Shell-core-shell Structure. In this structure, the magnetic iron oxide nanoparticles are located between two functional semiconductor materials. Several applications require magnetic iron oxide nanoparticles to be embedded in the nonmagnetic layers to avoid aggregation and sedimentation of

magnetic iron oxide nanoparticles as well as to endow them with particular surface properties for specific application. In this structure, the two shell layers use the same or different semiconductors or one layer is a non-semiconductor material.[75]

More importantly, understanding the relationship between the photocatalytic performance and the microstructures is a prerequisite for widespread applications. Therefore, design and controllable synthesis of the nanostructured photocatalysts, and further optimization of the microstructure and photocatalytic performance are still under broad investigation.[76] Prerequisite for every possible applied structure is the proper surface properties of such magnetic composite NPs, which determine their interaction with environment. These interactions ultimately affect the colloidal stability and photocatalytic efficiency of the composite particles.

2.4 Charge transfer mechanism

The charge separation mechanism in both capped semiconductor systems and coupled semiconductor systems involves the photoinduced electrons in one semiconductor being injected into the lower lying CB of the second semiconductor. Therefore, coupling semiconductors techniques do not always improve the photocatalytic performance by charge separation. The design of coupling semiconductors photocatalysts depends on the band structures of each component. Generally, photogenerated electronic on the CB of a higher level semiconductor are injected into the CB of lower level semiconductor. As such coupled semiconductor photocatalytic systems bear great hope for next-generation solar energy harvesting and advancing environmental remediation techniques. Governments and researchers have devoted considerable interests and resources to such fabrication, characterization, and optimization.[77]

In iron oxide-semiconductor system, the iron oxides can be a narrow band gap semiconductor, the band gap value of Fe_2O_3 is about 2.2 eV, and absorb the visible light. For example, the work

function (ϕ) of α- Fe_2O_3 is 5.88 eV, which is higher than most common wide band gap semiconductors (TiO_2 is 3.87 eV, ZnO is 4.35 eV, SnO_2 is 4.3 eV, WO_3 is 5.24 eV, etc.). As shown in **Figure 4a**, the band configuration and photogenerated charge carriers separations at interface of iron oxide/semiconductor (wide band gap) under light irradiation are proposed. Under light irradiation, the photoinduced electrons and holes are separated at the interface of iron oxide/semiconductor, the photoinduced electrons in CB of iron oxide tend to transfer to that the CB of semiconductor due to the decreased potential energy, and hence the coupling structure reduces the electron-hole recombination probability and increases the electron mobility. Thereby the electrons and holes were transferred to the surface of iron oxide and semiconductor, respectively, and finally form hydroxyl radicals (·OH). The superoxygen radicals ($\cdot O_2$) are formed by the combination of electrons with O_2 adsorbed on the surface of semiconductor. As a powerful oxidant, ·OH can degrade many pollutes, such as organic dyes, wastewater, plastics. However, capped semiconductors on the other hand have a core and shell geometry, as shown in **Figure 4b**. The electrons are injected into the energy levels of the core semiconductor (on condition that it has a conduction band potential which is lower than that of the shell). Hence, the electrons are trapped within the core particle, and is not readily accessible for the reduction reaction.[78]

Introduction of interlayer into the iron oxide-semiconductor heterojuction for tailoring the photocatalytic efficiency is another option. As shown in **Figure 5**, when the insulator SiO_2 layer is introduced, the photogenerated electrons in CB of iron oxide are not able to transfer to the CB of semiconductor. However, form our previous reports and Christopher's reports, the photogenerated electrons can still transfer if the thickness of SiO_2 is less than 5 nm. [79, 80] Therefore, the thickness of SiO_2 is a key factor and responsible for the photocatalytic abilites of iron oxide-SiO_2-semiconductor system. As an alternative, photogenerated electrons in CB of iron oxide

can transfer to the CB of semiconductor via a carbon interlayer, which behave as an electron conductor to enhance the electron-hole separation. For example, Hou and co-workers have reported an interlayer of graphene that transfer the electrons from the CB of $BiV_{1-x}Mo_xO_4$ shell to the CB of Fe_2O_3 core in α-Fe_2O_3 nanorod/graphene/ $BiV_{1-x}Mo_xO_4$ core/shell heterojunction due to band alignment and potential difference, which provide a direct path for electron transport.[81]

As a classical heterostructure, the iron oxide-semiconductor system has many advantages. First of all, the built-in potential at the interface of iron oxide and semiconductor can promote the separation and transport of photoinduced charge carriers. Second, iron oxides with relatively smaller band gap sensitizes the wide band gap semiconductors. Third, semiconductor metal oxides and metal sulfides such as RuO_2, NiO and IrO_2, MoS_2 and cobalt phosphates, can also act as effective co-catalysts to facilitate the surface electrochemical reaction. These co-catalysts improve charge separation, suppress the recombination of photogenerated charge carriers and lower the potential for electrochemical reaction.[14] Although α-Fe_2O_3 is stable, it is prone to photocorrosion. Its photocatalytic degradation efficiency for organic dyes needs to be improved. Therefore, as an outer layer, semiconductors such as TiO_2 with excellent electrochemical- and photochemical-stability can be used on the surface of iron oxide to improve the stability of the catalysts.

3 Synthesis of Magnetic Iron Oxide-Semiconductor Composite Nanomaterials

3.1 Seed-mediated Growth Strategy

As shown in **Figure 6a**, the seed-mediated growth strategy is the most common method for synthesizing high-quality magnetic iron oxide-semiconductor composite nanomaterials, especially the preparation of core-shell heterostructures. A typical growth protocol involves the addition of magnetic iron oxide nanoparticles, as seeds, to the bulk semiconductor growth. The growth solution is obtained by the reduction of semiconductor precursors. In this protocol, seeds are sequentially

added to growth solution in order to control the rate of heterogeneous deposition and thereby the rate of crystal growth. Many wet-chemical approaches have been used to generate the iron oxide-semiconductor composite heterostructures, such as co-precipitation method, hydrothermal method, solvothermal method, etc.[82-85]

For example, Chiu and co-workers have reported the synthesis of Fe_3O_4/ZnO core/shell nanoparticles by seed-meditated growth method in a nonhydrolytic condition. Control over thermal pyrolysis of zinc acetate renders a condition to overgrow ZnO layer on the surface of Fe_3O_4 seeds. This core/shell nanocrystals were magnetically separated by a 0.6 T magnet, which shows high potential of using such nanocrystals as recoverable catalyst material.[86] We proposed a facile pathway to prepare three different types of magnetic iron oxides/TiO_2 hybrid nanoparticles by seed-mediated method. The hybrid nanoparticles are composed of spindle, hollow, and ultrafine iron oxide nanoparticles as seeds and 3-aminopropyltriethyloxysilane as linker between the magnetic cores and TiO_2 layers, respectively. About 50% to 60% of MB was decomposed in 90 min in the presence of magnetic hybrid nanoparticles, which is higher than pure TiO_2 nanoparticles. The synthesized magnetic hybrid nanoparticles display high photocatalytic efficiency and can be used for cleaning polluted water with the help of magnetic separation.[87] Recently, Li and co-workers have reported a versatile kinetics-controlled coating approach to fabricate homogeneous porous TiO_2 shells for multi-functional core-shell nanostructures. By simply controlling the kinetics of hydrolysis and condensation of tetrabutyl titanate (TBOT) in ethanol/ammonia mixtures, the core-shell heterostructure with homogeneous porous TiO_2 shells were fabricated with variable diameter, geometry, and composition as seeds (e.g., α-Fe_2O_3 ellipsoids, Fe_3O_4 spheres, SiO_2 spheres, graphene oxide sheets, and carbon spheres). This approach exhibits many advantages, such as facile, reproducible and the thickness of TiO_2 shells can be tailored from 0 to 25, 45, and 70 nm.[88] Yuan

and co-workers have prepared Fe_3O_4@TiO_2 nanoparticles (the size is 6.7± 2.9 nm) by a modified sol-gel method. TiO_2 shell was formed by gradual adding the $TiCl_4$ to iron oxide nanoparticle gel. The as-prepared composite nanoparticles is used for targeted drug delivery.[89]

In addition, the semiconductor nanoparticles can also be seeds for the synthesis of iron oxide-semiconductor composite nanomaterials, and this strategy is often employed to fabricate the iron oxide/semiconductor with Janus structure (**Figure 6b**). For instance, Buonsanti and co-workers developed a colloidal seeded-growth strategy to synthesize all-oxide semiconductor/magnetic hybrid nanocrystals in various topological arrangements, in which the dimensions of the constituent material domains were controlled independently over a wide range. The Fe_xO_y/TiO_2 composite nanorods were synthesized by using the brookite TiO_2 nanorods as seeds and the $Fe(CO)_5$ as iron precursor *via* high-temperature thermal decomposition method. The preliminary magnetic and photocatalytic investigations had highlighted that the creation of bonding heterojunctions leads to significantly modified or even unexpected physical-chemical behaviour, relative to that offered by brookite TiO_2 and Fe_xO_y alone.[90, 91] Zeng and co-workers have first synthesized the TiO_2 nanoparticles with about 5-10 nm with ferric acetylacetonate as an iron source, the multifunctional Fe_3O_4-TiO_2 nanocomposites with Janus structure were prepared by the solvent-thermal method.[73] Liu and Gao first prepared the sheet-like TiO_2 seeds by hydrothermal treatment of TiO_2 nanoparticles. Then the α-Fe_2O_3/TiO_2 composite nanosheets were fabricated by hydrothermal treatment of ferric nitrate and hydroxylamine. Results showed that the photocatalytic activities of α-Fe_2O_3 make the MB degradation efficient under visible light irradiation.[92] Wang and co-workers synthesized one-dimensional (1D) heterostructures of uniform CdS nanowires separately decorated with hematite (α-Fe_2O_3) nanoparticles or magnetite (Fe_3O_4) microspheres via a two-step solvothermal deposition method. Each CdS nanowire had a uniform diameter of 40-50 nm and a length ranging to several

tens of micrometers. Quasicubic α-Fe_2O_3 nanoparticles with edge lengths up to 30 nm, and Fe_3O_4 microspheres with diameters of about 200 nm produced 1D dimer-type CdS/α-Fe_2O_3 semiconductor heterostructures or CdS/Fe_3O_4 semiconductor magnetic functionally assembled heterostructures. In comparison with the bare CdS nanowires and commercial anatase TiO_2, enhanced photocatalytic activity was observed in CdS/α-Fe_2O_3 heterostructures.[93]

3.2 Step-by-Step Deposition Strategy

Step-by-step deposition strategy is mainly used to prepare iron oxide-semiconductor composite multi-shells structure.[94-96] In fact, the need for a better control over surface properties or to protect the iron oxide itself, an interlayer was introduced in the magnetic iron oxide-semiconductor system to form multi-shell structure, as shown in **Figure 7**.[97-99] The most commonly used interlayer materials are the SiO_2 and carbon, respectively. Additionally, the interlayer can be removed by chemical corrosion or calcination.[70]

Silica coating can enhance the dispersion in solution because silica layer could screen the magnetic dipolar attraction between magnetic iron oxide nanoparticles, and hence increasing the stability of iron oxide nanoparticles and protect them in acidic environments. Silica have become the most used interlayer material.[100, 101] For example, Cheng and co-workers have synthesized Fe_3O_4@SiO_2@CeO_2 microspheres with magnetic core and mesoporous shell by step-by-step deposition strategy. Such multifunctional materials were utilized to capture phosphopeptides and catalyze the dephosphorylation simultaneously, thereby labeling the phosphopeptides for rapid identification.[102] Sarkar and co-workers have first synthesized the Fe_3O_4 nanoparticles with the diameter of 20 -40 nm by co-precipitation method, and then a SiO_2 interlayer was deposited on the surface of Fe_3O_4 nanoparticles by classical Stöber method. The Fe_3O_4/SiO_2/ZrO_2 composite nanoparticles were finally fabricated by reducing the $ZrOCl_2$ precursor. The thickness of ZrO_2 was

about 8 -10 nm, and the BET surface area of composite nanoparticles was up to 107 m^2g^{-1} due to the mesoporous ZrO_2 shell.[103] More recently, Chi and co-workers have prepared Fe_3O_4@SiO_2@TiO_2-Ag nanocomposite by step-by-step deposition strategy, the as-prepared microspheres show a number of important features as a recyclable photocatalyst: it contains a high field-responsive magnetic Fe_3O_4 core for efficient magnetic separation, a SiO_2 interlayer for protecting the Fe_3O_4 core from chemical- and photocorrosion, and a TiO_2 nano-shell with well dispersed Ag nanoparticles for enhanced photocatalytic activity.[104]

Like as SiO_2 interlayer, hydrophilic carbon coating on iron oxide nanoparticle core also endows better dispersibility and stability. More importantly, carbon coated iron oxide nanoparticles have been recently triggered enormous research activities due to the good chemical and thermal stability. The intrinsic high electrical conductivity of the carbon interlayer helps to transfer the electrons.[105-107] For instance, Qi and co-workers first deposited a carbon interlayer on the surface of Fe_3O_4 seeds by hydrothermal reaction of glucose, and then depositing SnO_2 on the surface of Fe_3O_4/C, they successfully obtained Fe_3O_4/C/SnO_2 composite nanoparticles.[108] Shi and co-workers have prepared a core/multi-shell-structured Fe_3O_4/C/TiO_2 magnetic photocatalyst by vapor phase hydrolysis process, and the photocatalytic abilities for degradation of methylene blue are studied. Compare with the commercial anatase TiO_2, Fe_3O_4/C/TiO_2 with low TiO_2 content (37%) exhibited a relatively higher photocatalytic activity. The C interlayer prevent the photocorrosion of Fe_3O_4 effectively, and the composite nanoparticles present a well magnetic recycling property due to magnetic core materials.[109] Liu and co-workers have fabricated the one-dimensional Fe_3O_4/C/CdS coaxial nanochains by a magnetic field-induced assembly and microwave-assisted deposition method. First, one-dimensional pearl chain-like Fe_3O_4/C core-shell nanocables were successfully assembled via the hydrothermal reaction of nanoscale Fe_3O_4 spheres with glucose in water in the

presence of an external magnetic field. The carbonaceous layer was about 10 nm in thickness, and it acted as the stabilizer for the Fe_3O_4 nanochains. Afterwards, CdS nanoparticles were facile deposited on Fe_3O_4/C nanochains by a rapid microwave-irradiation route to generate Fe_3O_4/C/CdS coaxial nanochains. The subsequently photocatalytic test for organic pollutants demonstrate that these magnetic composite possess enhanced photocatalytic activity as a MRPs under visible light irradiation. The decolorization fraction using the sample of microwave irradiation was up to 94.7% in 20 min, and the photocatalytic performance was still stable after 12 cycles of degradation of RhB, the results revealed that this MRPs possess excellent stability.[107]

3.3 Other Strategies

Except the above two conventional strategies, some new synthesis or preparation methods have also been used to fabricate the iron oxide-semiconductor composite nanomaterials, such as ion implantation method, spray pyrolysis, microwave, and sonochemical method.[110-112]

As shown in **Figure 8**, we first dropped the hematite seeds onto the surface of clean slide and implanted Ti ions, and finally magnetic monodisperse TiO_2 grains filled into spindle-like hematite bi-component nanoparticles were successfully synthesized.[113] Different implanted energy and the magnetic properties of bi-component α-Fe_2O_3/TiO_2 nanoparticles were investigated. The results illustrate α-Fe_2O_3/TiO_2 composite nanoparticles could be obtained by Ti ions implantation with different energy, and the saturation magnetization (M_S) of the samples after ion implantation were significantly enhanced.[114] Li and co-workers prepared a novel core–shell α-Fe_2O_3/SnO_2 heterostructure by a one-step flame-assisted spray pyrolysis of iron and tin precursor. The effect of SnO_2 component was investigated for the evolution of phase composition and morphology in detail. It was found that the doping of SnO_2 in Fe_2O_3 could effectively promote the phase transition from γ-Fe_2O_3 to α-Fe_2O_3 during flame synthesis. The unique morphology composed of tin doped α-Fe_2O_3

core and SnO_2 as a shell was attributed to the solubility, segregation and second-phase surface nucleation of SnO_2 in Fe_2O_3.[115]

4 Progress on the magnetic iron oxide-semiconductor composite photocatalysts

4.1 Magnetic iron oxide-metal oxide semiconductor composite photocatalysts

4.1.1 Magnetic iron oxide -TiO_2 photocatalysts

TiO_2, the semiconductor most thoroughly investigated in the literature, seems to be the most promising photocatalytic material for the destruction of organic pollutants. This semiconductor provides the best compromise between catalytic performance and stability in aqueous media. Therefore, the magnetic iron oxide-TiO_2 composite photocatalyst have become the research focus in recent years. Using magnetic properties of the iron oxide itself for obtaining the magnetic recoverable photocatalyst have become an important issue in the magnetic iron oxide-TiO_2 composite photocatalyst system.[116-119] For instance, Wang and co-workers have reported the fabrication of core-shell Fe_3O_4@SiO_2@TiO_2 microspheres through a wet-chemical approach. The microspheres possess both ferromagnetic and photocatalytic properties. The TiO_2 nanoparticles on the surfaces of microspheres degraded organic dyes under the illumination of UV light. Furthermore, the microspheres were easily separated from the solution after the photocatalytic process due to the ferromagnetic Fe_3O_4 core. The photocatalysts were recycled for further use and the degradation rate of methyl orange still reached 91% after 6 cycles of reuse.[120] As shown in **Figure 9**, Chalasani and Vasudevan have demonstrated water-dispersible photocatalytic Fe_3O_4@TiO_2 core-shell magnetic nanoparticles by anchoring β-cyclodextrin (CMCD) cavities to the TiO_2 shell, and they photocatalytically destroyed endocrine-disrupting chemicals, bisphenol A (BPA) and dibutyl phthalate, present in water. The particles, which were typically 12 nm in diameter, were magnetic

and removed from the dispersion by magnetic separation and reused. The concentration of BPA solution was determined by liquid chromatography, and then irradiated under UV light for 60 min. After photodegradation of BPA, the CMCD-Fe_3O_4@TiO_2 nanoparticles that were separated from the mixtures by a magnet, the recycled products can be reused for the photodegradation of newly prepared BPA solutions. The recycle photocatalytic performance of CMCD-Fe_3O_4@TiO_2 for the photodegradation of BPA was excellent and stable, retaining 90% efficiency after 10 cycles.[121] For obtaining the magnetic recovery photocatalysts, the Fe_3O_4 and γ-Fe_2O_3 were often employed due to their higher saturation magnetization and good magnetic separation ability.

On the other hand, the α-Fe_2O_3 has often been introduced in the magnetic iron oxide-TiO_2 composite photocatalyst in order to use its properties of narrow band gap, and to obtain magnetic iron oxide-TiO_2 composite heterostructures.[92, 122-124] For example, Peng and co-workers have synthesized Fe_2O_3/TiO_2 heterostructural photocatalysts by impregnation of Fe^{3+} on the surface of TiO_2 and annealing at 300 °C, the composites possess different mass ratios of Fe_2O_3 vs TiO_2. The photocatalytic activities of Fe_2O_3/TiO_2 heterocomposites, pure Fe_2O_3 and TiO_2 were studied by the photocatalytic degrading of Orange II dye in aqueous solution under visible light (λ > 420 nm) irradiation. The Fe_2O_3/TiO_2 heterogeneous photocatalysts exhibited an enhanced photocatalytic ability for Orange II, higher than either pure Fe_2O_3 or TiO_2. The best photocatalytic performance for Orange II could be obtained when the mass ratio is 7:3 in Fe_2O_3/TiO_2. The results illustrate that the generation of heterojunctions between Fe_2O_3 and TiO_2, that is key for improving the movement and restraining the recombination of photoinduced charge carriers, and finally improve the photocatalytic performance of Fe_2O_3/TiO_2 composites.[125] Recently, Palanisamy and co-workers have prepared Fe_2O_3/TiO_2 (10, 30, 50, 70 and 90 wt% Fe_2O_3) photocatalysts by sol–gel process. Mesoporous Fe_2O_3/TiO_2 composites exhibited excellent photocatalytic degradation ability for 4-chlorophenol in

aqueous solution under sunlight irradiation. The author claimed that the photogenerated electrons in the VB of TiO_2 are transferred to Fe (III) ions resulting in the reduction of Fe (III) ions to Fe (II) ions. Thus the photoinduced holes in the VB of Fe_2O_3/TiO_2 cause oxidation reaction and decompose the 4-chlorophenol to CO_2 and H_2O. Meanwhile the transferred electrons in Fe (III) ions could trigger the reduction reaction.[126]

4.1.2 Magnetic iron oxide -SnO_2 photocatalysts

As an n-type wide-bandgap semiconductor (~3.8 eV), tin oxide (SnO_2) has proved to be a material of exceptional technological importance due to its unique properties, including high stability and lithium storage capacity, and it is currently used to prepare photocatalysts. The objectives of combining the magnetic iron oxide and SnO_2 are the same with the iron oxide-TiO_2 composite photocatalyst system.

One hand is the fabrication of iron oxide/SnO_2 heterostructures, for instance, Niu and co-workers have prepared branched SnO_2/α-Fe_2O_3 semiconductor nanoheterostructures (SNHs) of high purity by a low-cost and environmentally friendly hydrothermal strategy, through crystallographic-oriented epitaxial growth of SnO_2 nanorods on α-Fe_2O_3 nanospindles and nanocubes, respectively (**Figure 10**). SnO_2/α-Fe_2O_3 SNHs exhibited excellent visible light or UV photocatalytic abilities, remarkably superior to their α-Fe_2O_3 precursors, mainly owing to the effective electron-hole separation at the SnO_2/α-Fe_2O_3 interface.[127] Recently, Zhang and co-workers have also synthesized the three-dimensional SnO_2/α-Fe_2O_3 semiconductor hierarchical nanoheterostructures via crystallographic-oriented epitaxial growth of SnO_2 onto the surface of flowerlike three-dimensional iron oxide hierarchical nanostructures. For this photocatalyst, visible-light-active flowerlike Fe_2O_3 hierarchical nanostructures were employed as a medium to harvest the visible light and generated photoinduced charge carriers, and SnO_2 layer was employed as charge collectors to transport the

photoinduced charge carriers. The SnO_2/α-Fe_2O_3 semiconductor hierarchical heterostructures present admirable visible-light photodegradation ability for organic dye of methylene blue, which could be assigned to the wide visible-light absorption range, high surface area, and efficient charge carriers separation of the SnO_2/α-Fe_2O_3 heterostructures.[128] Zhu and co-workers have synthesized the core-shell structured α-Fe_2O_3@SnO_2 shuttle-like composites via a facile solvothermal approach. The photocatalytic activities of the as-synthesized α-Fe_2O_3@SnO_2 core-shell shuttle-like composites were studied by the photodegradation of RhB dye under UV light irradiation (λ = 365 nm), and the absorption peak of RhB diminished gradually as the exposed time extended and completely disappeared after 70 min. Compared with uncoated α-Fe_2O_3 shuttle-like nanorods, SnO_2 nanoparticles, and the mixture of α-Fe_2O_3 nanorods and SnO_2 particles, as-synthesized core-shell shuttle-like composites exhibited enhanced photodegradation abilities, suggesting that the synergy effect of α-Fe_2O_3 and SnO_2 was beneficial to improve the photocatalytic activity.[129]

On the other hand, fabrication of magnetic recovery iron oxide-SnO_2 composite photocatalyst system is also attractive for various reasons. As shown in **Figure 11**, we have successfully synthesized the spindle-like and spherical iron oxide-SnO_2 composite nanoparticles via seed-mediate growth strategy recently, and the as-prepared iron oxides/SnO_2 core-shell heterostructures displayed enhanced visible light and UV photodegradation activity for RhB, which is significant higher than the uncoated a-Fe_2O_3 seeds and commercially available SnO_2 products. Significantly, the composite nanoparticles can be magnetically separated from the dispersion after the photocatalytic degradation.[130, 131] Zhang and co-workers have fabricated superparamagnetic iron oxide (SPIO)/SnO_2 yolk-shell heterostructures (YSHs) by a facile template approach, the as-obtained SnO_2 shell is mesoporous, the thickness of shell layer and void spaces are both tailorable. Under the UV light irradiation for 1 h, the photodegradation activity of as-obtained SPIO@SnO_2 YSHs and

commercial P25 TiO_2 for RhB were about 75% and 97%, respectively. Because of the SPIO cores are not photocatalytic active, the mass of SnO_2 component in 25 mg of SPIO@SnO_2 YSHs would be less than the photocatalyst component in the same mass of P25 TiO_2.[132]

4.1.3 Magnetic iron oxide -ZnO photocatalysts

Indeed, the photocatalytic performance of pure ZnO nanomaterials is not weaker than the TiO_2. However, it is unstable under illuminated aqueous solutions with $Zn(OH)_2$ being formed on the particle surface and results in catalyst deactivation. Owing to the photocatalytic performance of ZnO, the ZnO based composite nanomaterials are still used in the photocatalytic field and attracts more attention in recent years.[133-135] For instance, Liu and co-workers have synthesized the magnetic nest-like γ-Fe_2O_3/ZnO double-shelled hollow nanostructures *via* a step-by-step process. This interesting nest-like heterostructures consist of nanoscale ZnO flakes which grown on the surface of spherical γ-Fe_2O_3 particles. Significantly, these magnetic hollow heterostructures exhibited enhanced photodegradation ability for different organic dyes, including MB (almost 95.2% of MB could be degraded within 50 min), RhB (almost 91.1% of RhB could be degraded within 50 min), and MO (almost 82.5% of MO could be degraded within 80 min), and their photocatalytic abilities were higher than the commercial ZnO nanoparticles. The improved photodegradation ability of γ-Fe_2O_3/ZnO might be attributed to the large surface area comes from the nest-like hollow structure. The photodegradation performance of as-prepared γ-Fe_2O_3/ZnO heterostructures was still stable after 6 cycles without significant deterioration, suggesting that these γ-Fe_2O_3/ZnO heterostructures were highly stable and could be reused many times.[136] As shown in **Figure 12**, we have successfully fabricated mesoporous spindle-like α-Fe_2O_3/ZnO core-shell heterostructures by a surfactant-free, low-cost, and environmentally friendly seed-mediate strategy with the help of post-annealing treatment. The thickness of ZnO layer was

tailored by adjusting the concentration of zinc precursor. Considering that both α-Fe_2O_3 and ZnO are good photocatalytic materials, the photocatalytic activity of the core-shell heterostructures for organic dye RhB had been studied. It is noteworthy that the as-prepared α-Fe_2O_3/ZnO core-shell heterostructures displayed enhanced photodegradation performance, clearly higher than the uncoated α-Fe_2O_3 seeds and commercial P25 TiO_2, which mainly attributing to the synergistic effect between the narrow and wide bandgap semiconductors and effective photogenerated charge carries separation at the interface of α-Fe_2O_3 /ZnO.[137]

4.1.4 Others

Except the TiO_2, SnO_2 and ZnO, WO_3, ZrO_2, Cu_2O and Bi_2O_3 have also been investigated as a potential photocatalyst however, it is generally less photocatalytically active than TiO_2, and their semiconductor oxides have been used to functionalize the magnetic iron oxide nanoparticles.[138, 139] As shown in **Figure 13**, Xi and co-workers have synthesized a magnetically recyclable Fe_3O_4/WO_3 core-shell visible-light photocatalyst by a facile solvothermal epitaxial growth combined with a mild oxidation route. Photoelectrochemical investigations verified that the core-shell structured Fe_3O_4/WO_3 had more effective photoconversion capability than pure WO_3 or Fe_3O_4. At the same time, the visible-light photocatalytic ability of the Fe_3O_4/WO_3 photocatalyst exhibited significant enhancement in photodegradation of RhB. Furthermore, the Fe_3O_4/WO_3 core–shell photocatalyst was effectively recycled at least three times without an apparent decrease in its photocatalytic activity, which demonstrates its high stability.[140] Li and co-workers have successfully synthesized magnetic Fe_3O_4@C@Cu_2O composites with a bean-like core/shell nanostructure by step-by-step self-assembly. The carbonaceous layer with unavoidable hydrophilic groups inherited from the starting materials acted as both linker and stabilizer between Fe_3O_4 and Cu_2O. The Fe_3O_4@C@Cu_2O composites exhibited ferromagnetic behaviour, and good dispersibility

in aqueous solution. Importantly, the bean-like core/shell composites showed universal and powerful visible-light-photocatalytic activity for the degradation of RhB, methyl orange (MO), and alizarin red (AR) relative in comparison with commercial Cu_2O and Degussa P-25 powders.[141] Wang and co-workers have synthesized three-dimensional flowerlike hierarchical Fe_3O_4@Bi_2O_3 core-shell architecture by a facile solvothermal approach. The diameter of as-obtained flowerlike hierarchical microsphere was ca. 420 nm and the shell was composed of several nanosheets with a thickness of 4–10 nm and a width of 100-140 nm. The saturation magnetization of the superparamagnetic composite heterostructures was ca. 41 emu g^{-1} at room temperature. Additionally, the Fe_3O_4@Bi_2O_3 composite heterostructures exhibited much higher (7-10 times) photocatalytic ability than commercial Bi_2O_3 particles under visible-light irradiation. The photocatalytic activity of Fe_3O_4@Bi_2O_3 composite heterostructures did not display clear loss for the photocatalytic degradation of RhB after 6 recycles.[142]

Recently, new semiconductor oxides have been used in photocatalytic application, such as V_2O_5,[143] Nb_2O_5,[144, 145] Ta_2O_5,[146, 147] CeO_2,[148, 149] Ga_2O_3,[150] *etc.*[151] However, reports on the synthesis of magnetic iron oxide-semiconductor oxides are very scarce so far, and it is worth studying on various ways to introduce semiconductor oxides into iron oxide-semiconductor system and to improve the photocatalytic ability.

4.2 Magnetic iron oxide-metal chalcogenides semiconductor composite photocatalysts

Currently, the proportion of using semiconductor oxides in photocatalysts is large, however, the semiconductor sulfides such as ZnS, CdS, Bi_2S_3, SnS_2, ZnSe, etc. have also been attractive due to the importance of their special quantum confinement effect. [93, 152-156] As a competitive alternative, the application of magnetic iron oxide-semiconductor sulfides is a relatively new technology. The optical properties and photocatalytic performance of semiconductor sulfides could

be different from their oxide counterparts.

For example, Liu and co-workers have reported the preparation of Fe_3O_4/CdS nanocomposites via a sonochemical route in an aqueous solution. These Fe_3O_4/CdS nanocomposites displayed fluorescence and exhibited excellent magnetic properties at room temperature. Photocatalytic activity studies confirmed that as-prepared nanocomposites had high photocatalytic activity towards the photodegradation of methyl orange in aqueous solution. Furthermore, the photodecomposition rate decreased slightly after 12 cycles of photocatalysis (89% of MO is decomposed in the last cycle).[157] Their subsequent studies revealed that the Fe_3O_4/ZnS had high photocatalytic activity towards the photodegradation of eosin Y in aqueous solution. The catalytic efficiency only decreased by 5% after 15 cycles.[112] As shown in **Figure 14**, Shi and co-workers have synthesized α-Fe_2O_3/CdS cornlike nanocomposites via CdS nanoparticles by a simple one-step wet-chemical route, in which preformed single-crystaline α-Fe_2O_3 nanorods were used as substances for growing CdS nanoparticles. The cornlike nanocomposites exhibited superior photocatalytic performance under visible light irradiation (86.7% of MB was degraded in 120 min) over the pure α-Fe_2O_3 nanorods and CdS nanoparticles. The enhanced performance is attributed to larger surface area of the cornlike structure, the crystalline nature of the materials and the synergy in light absorption and charge separation between α-Fe_2O_3 and CdS.[158] Luo and co-workers have developed a facile and rapid synthesis of urchin-shaped Fe_3O_4@Bi_2S_3 core-shell hierarchical structure through a sonochemical method. The as-prepared Fe_3O_4@Bi_2S_3 hierarchical core-shell structures showed excellent photocatalytic efficiency for the degradation of RhB and retained the photocatalytic activity after being recycled for five times with the help of an external magnetic field.[159]

Additionally, some ternary semiconductor sulfides have been used in the application of photocatalyst, such as $Zn_xCd_{1-x}S$, $ZnIn_2S_4$, $CuInS_2$, etc.[160-165] However, there is no literature

report on iron oxide- ternary semiconductor sulfides composite photocatalytic system. More importantly, the toxicity of the semiconductor sulfides should also be considered in practical application.

4.3 Multiple semiconductor shells photocatalysts

The synergetic effects of multiple semiconductor photocatalysts have been observed extensive in photocatalytic degradations. In core-shell-shell structures, the first semiconductor shell layer can offer special active-sites for the adsorption/reaction of reactants/reaction intermediates. The second semiconductor shell layer could also influence the overall band configuration via altering the bandgap absorption and to separate the photoinduced charge carriers. [166-168] Moreover, semiconductors with narrow band gap can expand the spectral response range. As shown in **Figure 15**, by introducing semiconductor heterojunction on the surface of magnetic iron oxide nanomaterials, magnetic recovery photocatalysts are obtained.[14, 169-171]

For example, Chen and co-workers have synthesized three types of ellipsoidal complex hollow structures with the shells assembled from anatase TiO_2 nanosheets with exposed (001) facets by utilizing silica-coated hematite (α-Fe_2O_3) nanospindles as the starting templates. As shown in **Figure 16**, the α-Fe_2O_3/SiO_2/SnO_2/TiO_2 can be prepared by hydrothermal deposition of SnO_2 layer on the surface of SiO_2. The Fe_3O_4@SnO_2@TiO_2 nanorattles manifested a much higher degradation efficiency compared to the Degussa P25 nanoparticles, as well as their analogous Fe_3O_4@TiO_2 core-shell nanomaterial without the exposed (001) high-energy facets.[172] Dong and co-workers have prepared the CdS modified TiO_2/Fe_3O_4 photocatalysts by sol-gel and immersion methods. The CdS-TiO_2/Fe_3O_4 composites exhibited higher photocatalytic activity than pure TiO_2 and TiO_2/Fe_3O_4 for the degradation of Reactive Brilliant Red X-3B dye (X-3B) under simulated sunlight. In addition, a gradual loss of photocatalytic activity was observed in reusability test of

$CdS\text{-}TiO_2/Fe_3O_4$ composites, and degradation of X-3B reached to 78.9 % after five runs.[173] Obviously, photocatalysts with multiple semiconductor shells can effectively improve the photocatalytic abilities.

5 Summary and Perspectives

Several fundamental issues must be addressed before the photocatalysts are economically viable for large scale industrial applications. Apart from offering easy separation of the photocatalysts from the reaction system, magnetic iron oxide-semiconductor photocatalytic system, which interfaces chemistry with materials science, possesses a unique position in the advancement of heterogeneous photocatalysis. **Table 1** depicts the representative magnetic iron oxide-semiconductor photocatalysts and their photocatalytic performances. Though a lot of effort has been made in design and fabricating magnetic iron oxide-semiconductor composite photocatalytic system, it is still a field of research in modern photocatalysis and following issues are still need to be addressed.

1) In order to improve the photocatalytic activities of photocatalysts, the extension of excitation wavelength, reduced charge carrier recombination, and the promotion of active sites around the surface should be considered. Therefore, if noble metal nanomaterials have been introduced in the magnetic iron oxide-semiconductor system, the photocatalytic efficiency could be enhanced. The photogenerated charge carriers in the noble metal can be separated by the metal/semiconductor heterojunction. Additionally, the separated electron and hole can take part in the chemical reactions on the surface of metal and semiconductor, respectively. The absorbed photons can excite the valence electrons of noble metal due to surface plasmon resonance (SPR) effect. The energy of photoinduced electrons is higher than Schottky barrier resulted in crossing the interface and transferring to the VB of the semiconductor. Numerous literature reports are dedicated to the metal/semiconductor composite photocatalytic system. However, the report on magnetic iron

oxide-noble metal-semiconductors ternary photocatalysts is scarce and necessary to be strengthened.[174] Owing to the SPR effect, solution processed metal nanoparticles coated onto the surface of iron oxide or semiconductors is an effective method to enhance the absorption of visible-light. However, the metal nanoparticles can also act as recombination centres resulting in inferior photocatalytic performance due to the incorporation of chemically synthesized metal nanoparticles in iron oxide-semiconductor composite system. Many factors can cause the undesirable exciton quenching and decreases the plasmonic effect. Indeed, coating of metal nanoparticles with insulating materials can prevent such recombination centres.[175] More recently, we have reported a novel iron oxide/noble metal/semiconductor ternary multilayer hybrid structure that were prepared by template synthesis and subsequent layer-by-layer deposition method. Three different morphologies of α-Fe_2O_3/Ag/SiO_2/SnO_2 heterosturctures were obtained, the thickness of insulating SiO_2 interlayer was tailored to control the coupling of noble metal silver with the tin oxide. The as-obtained α-Fe_2O_3/Ag/SiO_2/SnO_2 nanocomposites exhibited an enhanced catalytic abilities under UV or visible light irradiation, higher than the commercially available pure SnO_2, naked α-Fe_2O_3 seeds and α-Fe_2O_3/SnO_2 binary nanocomposites. Moreover, α-Fe_2O_3/Ag/SiO_2/SnO_2 exhibited significant stability and recyclability because of its photodegradation rate maintains at 96% after 8 cycles.[176]

(2) The fusion of catalysis with nanotechnology continues to generate better materials and improve their functions. Graphene and it use in photodegradation is one of the latest examples. Its interesting electrical and mechanical properties, and high surface area make graphene a novel substrate for forming hybrid structures with a variety of nanomaterials. The use of graphene to enhance the efficiency of photocatalysts has attracted much attention. Utilization of single-layer graphene sheets can not only provide a high quality two-dimensional photocatalyst support, but also a

two-dimensional circuit board, with an attractive potential to harness their perfect electrical and redox properties. There are few literature reports on composites of graphene with magnetic iron oxide-semiconductors photocatalytic system.[177]

(3) At present, a large number of fundamental and applied research of photocatalysis are focused on the synthesis and modification of new photocatalysts, nevertheless, with those endeavour, the effect of photocatalysts microstructure on their photocatalytic performance still cannot be understood, understanding the relationship between these two parts is a prerequisite for broad applications of composite nanomaterials in photocatalyst. However, the understanding of interface effects, coupling mechanism, photocatalyst life, deactivation and the regeneration mechanism are still relatively weak.[178] As a heterogeneous catalytic reaction system, the semiconductor photocatalytic materials would be deactivated in the practical application, such as the photocatalytic effiency of P25 TiO_2 becomes very low after 3 cycles under sunlight. Therefore, deactivation and the regeneration mechanism of semiconductor photocatalysts should be reinforced.

As a key issue for practical applications, the facile method to increase the photocorrosion suppression ability, the life and stability of magnetic iron oxide-semiconductor composite photocatalytic system must be further developed and improved. To date, the underlying photocorrosion mechanism for the iron oxide-semiconductor composite photocatalyst is not clear, and systematic studies are necessary. Many methods have been used to reduce the photocorrosion of pure semiconductors, such as graphene composites,[179] graphene oxide,[180] quantum dot,[181], etc, and these materials can be introduced in magnetic iron oxide-semiconductor composite photocatalytic system. Moreover, recycling and regeneration is also an effective method to extend the life of deactivated photocatalyst. However, reports on the above mentioned issues are scarce so far.

(4) Although a great effort has been made in the past years to unravel the mechanisms of bi-/ternary and multiple composite photocatalysts, it is still a challenge for various researchers. To develop an efficient heterostructural photocatalysis system for large-scale industrialization, understanding of the kinetics and mechanisms of these charge transfer processes is very important.[182] More efforts on photo-inducing charge carrier generation, trapping, recombination, and transporting need to further to strengthen and improve. Apart from the traditional characterization techniques, more and more photoelectrochemical methods and techniques have been used to study the kinetics and mechanisms of heterostructural photocatalysis systems. For instance, photoelectron spectroscopy (PES) is used to measure band bending in semiconductors, femtosecond transient reflecting grating (TRG) method is used to detect the photogenerated ultrafast relaxation dynamic at solid/liquid interfaces, O^2 photostimulated desorption (PSD) and electronstimulated desorption (ESD) is used to study the surface photoreactions induced by the photo-excited electrons and holes in the semiconductor, etc.[183-186] At present, charge transfer kinetics on a short duration is well studied, while the charge transfer on a more extended timescale is still unclear. Therefore, unravelling the mechanisms play an important and key role in magnetic iron oxide-semiconductor composite photocatalytic system. On this regard, there are several mechanisms are still not fully understanding and many works need to do.

(5) In fact, the photodegradation of pollutants is mainly used the suspension of semiconductor nanomaterials in this field. However, from a practical point of view, there are many limitations of using photocatalyst suspension, such as requirement of large photo-reactors, hard to filtrate the nanoscale photocatalyst, etc. Owing to the catalytic mechanism of these synthesized photocatalyst are very complicated, the pure semiconductors and α-Fe_2O_3/semiconductor composite photocatalytic systems are hardly recycled by extern magnetic field due to its weak magnetic response. As shown in

Figure 17, these photocatalysts can be printed on the rigid or flexible substrates as photocatalytic array or patterns, including screen printing,[187-189] offset printing,[190] inkjet printing,[191-193] gravure printing,[194] etc.[195, 196] These printed patterns with semiconductor photocatalysts can be also recycled. Therefore, combining and developing more practical methods to use these composite photocatalytic system should be further reinforced.

Acknowledgment

The author thanks the Hong Kong Scholars Program, NSFC (51471121, 51201115, 51171132), Young Chenguang Project of Wuhan City (2013070104010011), China Postdoctoral Science Foundation (2014M550406), Hubei Provincial Natural Science Foundation (2014CFB261) and the Fundamental Research Funds for the Central Universities.

Author Biography

Wei Wu obtained his B.S. in 2005 and M.S. in 2008 from Hunan University of Technology, and he received his PhD on *Materials Physics and Chemistry* in 2011 under the supervision of Prof. Changzhong Jiang in Department of Physics, Wuhan University, China. He then joined the group of Prof. Daiwen Pang at Department of Chemistry and Molecular Science, Wuhan University, for a postdoctoral fellow to design and synthesis of magnetic iron oxide-semiconductor heterostructures. Now he is the Director and Associate Professor of Laboratory of Printable Functional Nanomaterials and Printed Electronics, School of Printing and Packaging, Wuhan University. He has published, as an author and co-author, more than 60 publications in various reputed international journals. He is also the Associate Editor of *Journal of Nanoscience Letters*, and editorial board member of *Advanced Science, Engineering and Medicine* and *Journal of Green Science and Technology*, his research interests include the synthesis, properties, and application of nanomaterials, printed electronics and sensors.

Changzhong Jiang received his B.S in 1983 from Huazhong University of Science and Technology, M.S. in 1990 from Wuhan University. He obtained his PhD in 1999 from Université Claude Bernard Lyon 1, France. Currently, he is a full professor in Department of Physics, Wuhan University from 2001, and he is also the Director of Research Center of Ion Beam Materials, Wuhan University. He has published, as an author and co-author, more than 80 publications in various reputed international journals, such as *Physical Review Letters*, *Nano Letters*, *ACS Nano*, *Advanced Materials*, etc. His research interests include the synthesis and application of low-dimension nanomaterials, magnetic materials and ion beam materials.

Vellaisamy A. L.Roy obtained his Ph.D. degree from Nagpur University in 2004. Dr. Vellaisamy started his research on light-emitting materials for his Ph.D., mainly on Electron Spin Resonance analysis of organic materials

and was working on the growth of wide band gap nano-structures. Currently, he is an associate professor at the Department of Physics and Materials Science, City University of Hong Kong. His research interests are design, syntheses, and charge transport analysis of self-assembled nanostructures and functional materials for sensors, thin film transistors and floating gate flash memories. Dr. Vellaisamy received the TRIL Fellowship awarded by UNESCO in 2003 and an Excellent Product Award for his project prototypes on Sensors and Memories at China Hitech-Fair for three consecutive years since 2002. He has published over 80 papers in international SCI journals, including *Advanced Materials, Angewandte Chemie International Edition, Nano Letters*, *ACS Nano* and his papers have been cited for more than 1800 times.

References

[1] M.R. Hoffmann, S.T. Martin, W. Choi, D.W. Bahnemann, Chem. Rev. , 95 (1995) 69-96.
[2] X. Chen, S.S. Mao, Chem. Rev. , 107 (2007) 2891-2959.
[3] S. Liu, J. Yu, M. Jaroniec, Chem. Mater. , 23 (2011) 4085-4093.
[4] L. Sun, J.R. Bolton, J. Phys. Chem., 100 (1996) 4127-4134.
[5] T. Bak, J. Nowotny, M. Rekas, C.C. Sorrell, Int. J. Hydrogen Energy 27 (2002) 991-1022.
[6] A.C. Papageorgiou, N.S. Beglitis, C.L. Pang, G. Teobaldi, G. Cabailh, Q. Chen, A.J. Fisher, W.A. Hofer, G. Thornton, PNAS, 107 (2010) 2391-2396.
[7] L. Liu, Y. Li, Aerosol and Air Quality Research, 14 (2014) 453-469.
[8] J. Zhang, S. Chen, L. Qian, X. Tao, L. Yang, H. Wang, Y. Li, E. Zhang, J. Xi, Z. Ji, J. Am. Ceram. Soc. , (2014) n/a-n/a.
[9] D.J. Cole-Hamilton, Science, 299 (2003) 1702-1706.
[10] A. Kudo, Y. Miseki, Chem. Soc. Rev. , 38 (2009) 253-278.
[11] S.G. Kumar, L.G. Devi, J. Phys. Chem. A, 115 (2011) 13211-13241.
[12] A.H. Lu, E.L. Salabas, F. Schuth, Angew. Chem. Int. Ed., 46 (2007) 1222-1244.
[13] S. Laurent, D. Forge, M. Port, A. Roch, C. Robic, L.V. Elst, R.N. Muller, Chem. Rev. , 108 (2008) 2064-2110.
[14] Y. Qu, X. Duan, Chem. Soc. Rev. , 42 (2013) 2568-2580.
[15] P. Xu, G.M. Zeng, D.L. Huang, C.L. Feng, S. Hu, M.H. Zhao, C. Lai, Z. Wei, C. Huang, G.X. Xie, Z.F. Liu, Sci. Total Environ. , 424 (2012) 1-10.
[16] Y. Wang, Q. Wang, X. Zhan, F. Wang, M. Safdar, J. He, Nanoscale, 5 (2013) 8326-8339.
[17] W. Wei, Q.G. He, C. Hong, Prog Chem, 20 (2008) 265-272.
[18] W. Wu, Q.G. He, C.Z. Jiang, Nanoscale Res. Lett. , 3 (2008) 397-415.
[19] L. Zhou, J. Yuan, Y. Wei, J. Mater. Chem. , 21 (2011) 2823-2840.
[20] R.M. Cornell, U. Schwertmann, Wiley-VCH2003.
[21] M. Yamaura, R.L. Camilo, L.C. Sampaio, M.A. Macedo, M. Nakamura, H.E. Toma, J. Magn. Magn. Mater. , 279 (2004) 210-217.
[22] A. Demortiere, P. Panissod, B. Pichon, G. Pourroy, D. Guillon, B. Donnio, S. Begin-Colin, Nanoscale, 3 (2011) 225-232.
[23] W. Wu, X.H. Xiao, F. Ren, S.F. Zhang, C.Z. Jiang, J. Low Temp. Phys. , 168 (2012) 306-313.
[24] J. Choi, J. Cha, J.-K. Lee, RSC Adv., 3 (2013) 8365-8371.
[25] W. Wu, X.H. Xiao, S.F. Zhang, H. Li, X.D. Zhou, C.Z. Jiang, Nanoscale Res. Lett. , 4 (2009) 926-931.
[26] R. Massart, IEEE Trans. Magn., 17 (1981) 1247-1248.
[27] W. Wu, Q.G. He, R. Hu, J.K. Huang, H. Chen, Rare Met. Mater. Eng., 36 (2007) 238-243.
[28] S.K. Suh, K. Yuet, D.K. Hwang, K.W. Bong, P.S. Doyle, T.A. Hatton, J. Am. Chem. Soc. , 134

(2012) 7337-7343.
[29] J. Park, K. An, Y. Hwang, J.G. Park, H.J. Noh, J.Y. Kim, J.H. Park, N.M. Hwang, T. Hyeon, Nat. Mater. , 3 (2004) 891-895.
[30] J. Park, E. Lee, N.M. Hwang, M. Kang, S.C. Kim, Y. Hwang, J.G. Park, H.J. Noh, J.Y. Kim, J.H. Park, Angewandte Chemie, 117 (2005) 2932-2937.
[31] D. Amara, J. Grinblat, S. Margel, J. Mater. Chem. , 22 (2012) 2188-2195.
[32] W. Wu, X.H. Xiao, S.F. Zhang, J.A. Zhou, L.X. Fan, F. Ren, C.Z. Jiang, J. Phys. Chem. C 114 (2010) 16092-16103.
[33] W. Wu, X.H. Xiao, S.F. Zhang, T.C. Peng, J. Zhou, F. Ren, C.Z. Jiang, Nanoscale Res. Lett. , 5 (2010) 1474-1479.
[34] Y. Tian, B. Yu, X. Li, K. Li, J. Mater. Chem. , 21 (2011) 2476-2481.
[35] W.T. Dong, C.S. Zhu, J. Mater. Chem. , 12 (2002) 1676-1683.
[36] H. Qi, B. Yan, W. Lu, C. Li, Y. Yang, Current Nanoscience, 7 (2011) 381-388.
[37] K. Wongwailikhit, S. Horwongsakul, Mater. Lett. , 65 (2011) 2820-2822.
[38] L.-H. Han, H. Liu, Y. Wei, Powder Technol. , 207 (2011) 42-46.
[39] R. Ladj, A. Bitar, M. Eissa, Y. Mugnier, R. Le Dantec, H. Fessi, A. Elaissari, Journal of Materials Chemistry B, (2013).
[40] R. Abu Mukh-Qasem, A. Gedanken, J. Colloid Interface Sci. , 284 (2005) 489-494.
[41] R. Abu-Much, A. Gedanken, J. Phys. Chem. C 112 (2008) 35-42.
[42] A.L. Morel, S.I. Nikitenko, K. Gionnet, A. Wattiaux, J. Lai-Kee-Him, C. Labrugere, B. Chevalier, G. Deleris, C. Petibois, A. Brisson, M. Simonoff, Acs Nano, 2 (2008) 847-856.
[43] W. Wu, Q.G. He, H. Chen, J.X. Tang, L.B. Nie, Nanotechnology, 18 (2007) 145609.
[44] S.G. Zhang, Y. Zhang, Y. Wang, S.M. Liu, Y.Q. Deng, PCCP 14 (2012) 5132-5138.
[45] X. Hu, J.C. Yu, J. Gong, Q. Li, G. Li, Adv. Mater. , 19 (2007) 2324-2329.
[46] L.H. Wu, H.B. Yao, B. Hu, S.H. Yu, Chem. Mater. , 23 (2011) 3946-3952.
[47] Z. Ai, K. Deng, Q. Wan, L. Zhang, S. Lee, J. Phys. Chem. C, 114 (2010) 6237-6242.
[48] G. Qiu, H. Huang, H. Genuino, N. Opembe, L. Stafford, S. Dharmarathna, S.L. Suib, J. Phys. Chem. C, 115 (2011) 19626-19631.
[49] H. Vali, B. Weiss, Y.L. Li, S.K. Sears, S.S. Kim, J.L. Kirschvink, L. Zhang, PNAS 101 (2004) 16121-16126.
[50] A. Scheffel, M. Gruska, D. Faivre, A. Linaroudis, J.M. Plitzko, D. Schuler, Nature, 440 (2006) 110-114.
[51] D.A. Bazylinski, R.B. Frankel, Nat. Rev. Microbiol. , 2 (2004) 217-230.
[52] C. Pascal, J.L. Pascal, F. Favier, M.L. Elidrissi Moubtassim, C. Payen, Chem. Mater. , 11 (1998) 141-147.
[53] M. Starowicz, P. Starowicz, J. Żukrowski, J. Przewoźnik, A. Lemański, C. Kapusta, J. Banaś, J. Nanopart. Res. , 13 (2011) 7167-7176.
[54] G. Wang, Y. Ling, D.A. Wheeler, K.E.N. George, K. Horsley, C. Heske, J.Z. Zhang, Y. Li, Nano Lett. , 11 (2011) 3503-3509.
[55] G. Salazar-Alvarez, M. Muhammed, A.A. Zagorodni, Chem. Eng. Sci. , 61 (2006) 4625-4633.
[56] H.Y. Huang, Y.T. Shieh, C.M. Shih, Y.K. Twu, Carbohydr. Polym. , 81 (2010) 906-910.
[57] I. Morjan, R. Alexandrescu, F. Dumitrache, R. Birjega, C. Fleaca, I. Soare, C. Luculescu, G. Filoti, V. Kuncer, L. Vekas, J. Nanosci. Nanotechnol. , 10 (2010) 1223-1234.
[58] G. Martínez, A. Malumbres, R. Mallada, J. Hueso, S. Irusta, O. Bomatí-Miguel, J. Santamaría, Nanotechnology, 23 (2012) 425605.
[59] T. Thurston, J. Wilcoxon, J. Phys. Chem. B, 103 (1999) 11-17.
[60] W. Wu, S.F. Zhang, J. Zhou, X.H. Xiao, F. Ren, C.Z. Jiang, Chem-Eur J, 17 (2011) 9708-9719.

[61] I. Shakir, M. Shahid, D.J. Kang, Chem. Commun. , 46 (2010) 4324-4326.
[62] W. Wu, X.H. Xiao, T.C. Peng, C.Z. Jiang, Chem.-Asian J., 5 (2010) 315-321.
[63] W. Wu, X.H. Xiao, S.F. Zhang, J.A. Zhou, F. Ren, C.Z. Jiang, Chem. Lett. , 39 (2010) 684-685.
[64] D. Chen, F. Huang, G. Ren, D. Li, M. Zheng, Y. Wang, Z. Lin, Nanoscale, 2 (2010) 2062-2064.
[65] Q. Xiang, J. Yu, M. Jaroniec, Chem. Soc. Rev. , 41 (2012) 782-796.
[66] R. Vinu, G. Madras, J. Indian Inst. Sci. , 90 (2010) 189-230.
[67] L. Zhang, H. Cheng, R. Zong, Y. Zhu, J. Phys. Chem. C, 113 (2009) 2368-2374.
[68] T.T. Vu, L. del Río, T. Valdés-Solís, G. Marbán, Appl. Catal. B, 140–141 (2013) 189-198.
[69] J. Liu, J. Xu, R. Che, H. Chen, M. Liu, Z. Liu, Chemistry – A European Journal, 19 (2013) 6746-6752.
[70] W. Li, Y. Deng, Z. Wu, X. Qian, J. Yang, Y. Wang, D. Gu, F. Zhang, B. Tu, D. Zhao, J. Am. Chem. Soc. , 133 (2011) 15830-15833.
[71] Y. Luo, J. Luo, J. Jiang, W. Zhou, H. Yang, X. Qi, H. Zhang, H.J. Fan, D.Y.W. Yu, C.M. Li, T. Yu, Energy Environ. Sci. , 5 (2012) 6559-6566.
[72] C. Wang, L. Yin, L. Zhang, L. Kang, X. Wang, R. Gao, J. Phys. Chem. C, 113 (2009) 4008-4011.
[73] L. Zeng, W. Ren, L. Xiang, J. Zheng, B. Chen, A. Wu, Nanoscale, 5 (2013) 2107-2113.
[74] F. Mou, L. Xu, H. Ma, J. Guan, D.-r. Chen, S. Wang, Nanoscale, 4 (2012) 4650-4657.
[75] C. Wang, C. Xu, H. Zeng, S. Sun, Adv. Mater. , 21 (2009) 3045-3052.
[76] W. Wu, L. Liao, S.F. Zhang, J. Zhou, X.H. Xiao, F. Ren, L.L. Sun, Z.G. Dai, C.Z. Jiang, Nanoscale, 5 (2013) 5628-5636.
[77] R. Mohamed, D. McKinney, W. Sigmund, Materials Science and Engineering: R: Reports, 73 (2012) 1-13.
[78] I. Bedja, P.V. Kamat, Journal of Physical Chemistry, 99 (1995) 9182-9188.
[79] J. Zhou, F. Ren, S. Zhang, W. Wu, X. Xiao, Y. Liu, C. Jiang, J Mater Chem A, 1 (2013) 13128-13138.
[80] S. Linic, P. Christopher, D.B. Ingram, Nat. Mater. , 10 (2011) 911-921.
[81] Y. Hou, F. Zuo, A. Dagg, P. Feng, Nano Lett. , 12 (2012) 6464-6473.
[82] J. Zhang, X.H. Liu, L.W. Wang, T.L. Yang, X.Z. Guo, S.H. Wu, S.R. Wang, S.M. Zhang, Nanotechnology, 22 (2011) 185501.
[83] W. Yan, H. Fan, C. Yang, Mater. Lett. , 65 (2011) 1595-1597.
[84] L. Peng, T. Xie, Y. Lu, H. Fan, D. Wang, PCCP 12 (2010) 8033-8041.
[85] X. Yu, J. Wan, Y. Shan, K. Chen, X. Han, Chem. Mater. , 21 (2009) 4892-4898.
[86] W. Chiu, P. Khiew, M. Cloke, D. Isa, H. Lim, T. Tan, N. Huang, S. Radiman, R. Abd-Shukor, M.A.A. Hamid, C. Chia, J. Phys. Chem. C, 114 (2010) 8212-8218.
[87] W. Wu, X.H. Xiao, S.F. Zhang, F. Ren, C.Z. Jiang, Nanoscale Res. Lett. , 6 (2011) 533.
[88] W. Li, J. Yang, Z. Wu, J. Wang, B. Li, S. Feng, Y. Deng, F. Zhang, D. Zhao, J. Am. Chem. Soc. , 134 (2012) 11864-11867.
[89] Y. Yuan, S. Chen, T. Paunesku, S.C. Gleber, W.C. Liu, C.B. Doty, R. Mak, J. Deng, Q. Jin, B. Lai, K. Brister, C. Flachenecker, C. Jacobsen, S. Vogt, G.E. Woloschak, Acs Nano, 7 (2013) 10502-10517.
[90] R. Buonsanti, E. Snoeck, C. Giannini, F. Gozzo, M. Garcia-Hernandez, M.A. Garcia, R. Cingolani, P.D. Cozzoli, PCCP 11 (2009) 3680-3691.
[91] R. Buonsanti, V. Grillo, E. Carlino, C. Giannini, F. Gozzo, M. Garcia-Hernandez, M.A. Garcia, R. Cingolani, P.D. Cozzoli, J. Am. Chem. Soc. , 132 (2010) 2437-2464.
[92] H. Liu, L. Gao, J. Am. Ceram. Soc. , 89 (2006) 370-373.
[93] L. Wang, H. Wei, Y. Fan, X. Gu, J. Zhan, J. Phys. Chem. C, 113 (2009) 14119-14125.

[94] G. Schneider, G. Decher, Nano Lett. , 4 (2004) 1833-1839.
[95] Y. Wang, A.S. Angelatos, F. Caruso, Chem. Mater. , 20 (2007) 848-858.
[96] S. Srivastava, N.A. Kotov, Acc. Chem. Res. , 41 (2008) 1831-1841.
[97] Y. Li, J.S. Wu, D.W. Qi, X.Q. Xu, C.H. Deng, P.Y. Yang, X.M. Zhang, Chem. Commun. , (2008) 564-566.
[98] S. Abramson, L. Srithammavanh, J.-M. Siaugue, O. Horner, X. Xu, V. Cabuil, J. Nanopart. Res. , 11 (2009) 459-465.
[99] C. Wang, L. Yin, L. Zhang, L. Kang, X. Wang, R. Gao, J. Phys. Chem. C, 113 (2009) 4008-4011.
[100] T.A. Gad-Allah, K. Fujimura, S. Kato, S. Satokawa, T. Kojima, J. Hazard. Mater. , 154 (2008) 572-577.
[101] X. Huang, G. Wang, M. Yang, W. Guo, H. Gao, Mater. Lett. , 65 (2011) 2887-2890.
[102] G. Cheng, J.-L. Zhang, Y.-L. Liu, D.-H. Sun, J.-Z. Ni, Chem. Commun. , 47 (2011) 5732-5734.
[103] A. Sarkar, S.K. Biswas, P. Pramanik, J. Mater. Chem. , 20 (2010) 4417-4424.
[104] Y. Chi, Q. Yuan, Y. Li, L. Zhao, N. Li, X. Li, W. Yan, J. Hazard. Mater. , 262 (2013) 404-411.
[105] H. Wang, L. Sun, Y. Li, X. Fei, M. Sun, C. Zhang, Y. Li, Q. Yang, Langmuir, 27 (2011) 11609-11615.
[106] Y. Jing, C. Shi-Hai, L. Hong-Zhen, Chinese J Inorg Chem, 29 (2013) 2043-2048.
[107] Y. Liu, L. Zhou, Y. Hu, C. Guo, H. Qian, F. Zhang, X.W.D. Lou, J. Mater. Chem. , 21 (2011) 18359-18364.
[108] D.W. Qi, J. Lu, C.H. Deng, X.M. Zhang, J. Phys. Chem. C 113 (2009) 15854-15861.
[109] F. Shi, Y. Li, Q. Zhang, H. Wang, Int. J. Photoenergy 2012 (2012) 365401.
[110] H.-P. Peng, R.-P. Liang, L. Zhang, J.-D. Qiu, Electrochim. Acta 56 (2011) 4231-4236.
[111] Z. Wang, L. Wu, M. Chen, S. Zhou, J. Am. Chem. Soc. , 131 (2009) 11276-11277.
[112] X. Liu, Q. Hu, X. Zhang, Z. Fang, Q. Wang, J. Phys. Chem. C, 112 (2008) 12728-12735.
[113] L.L. Sun, W. Wu, S.F. Zhang, J. Zhou, G.X. Cai, F. Ren, X.H. Xiao, Z.G. Dai, C.Z. Jiang, AIP Adv., 2 (2012) 032179.
[114] L.L. Sun, W. Wu, S.F. Zhang, Y.C. Liu, X.H. Xiao, F. Ren, G.X. Cai, C.Z. Jiang, J. Nanosci. Nanotechnol. , 13 (2013) 5428-5433.
[115] Y. Li, Y. Hu, H. Jiang, X. Hou, C. Li, Crystengcomm, 15 (2013) 6715-6721.
[116] S. Xuan, W. Jiang, X. Gong, Y. Hu, Z. Chen, J. Phys. Chem. C, 113 (2008) 553-558.
[117] Q. Yuan, N. Li, W.C. Geng, Y. Chi, X.T. Li, Mater. Res. Bull. , 47 (2012) 2396-2402.
[118] Y.Z. Wang, X.B. Fan, S.L. Wang, G.L. Zhang, F.B. Zhang, Mater. Res. Bull. , 48 (2013) 785-789.
[119] B. Cui, H.X. Peng, H.Q. Xia, X.H. Guo, H.L. Guo, Sep. Purif. Technol. , 103 (2013) 251-257.
[120] Z. Wang, L. Shen, S. Zhu, Int. J. Photoenergy 2012 (2012) 202519.
[121] R. Chalasani, S. Vasudevan, Acs Nano, 7 (2013) 4093-4104.
[122] W. Zhou, H. Fu, K. Pan, C. Tian, Y. Qu, P. Lu, C.-C. Sun, J. Phys. Chem. C, 112 (2008) 19584-19589.
[123] F.-X. CHEN, W.-Q. FAN, T.-Y. ZHOU, W.-H. HUANG, Acta Phys. Chim. Sin. , 29 (2013) 167-175.
[124] W.S. Tung, W.A. Daoud, ACS Appl. Mater. Interfaces 1(2009) 2453-2461.
[125] L.L. Peng, T.F. Xie, Y.C. Lu, H.M. Fan, D.J. Wang, PCCP 12 (2010) 8033-8041.
[126] B. Palanisamy, C.M. Babu, B. Sundaravel, S. Anandan, V. Murugesan, J. Hazard. Mater. , 252–253 (2013) 233-242.
[127] M.T. Niu, F. Huang, L.F. Cui, P. Huang, Y.L. Yu, Y.S. Wang, Acs Nano, 4 (2010) 681-688.
[128] S.W. Zhang, J.X. Li, H.H. Niu, W.Q. Xu, J.Z. Xu, W.P. Hu, X.K. Wang, Chempluschem, 78

(2013) 192-199.
[129] L.-P. Zhu, N.-C. Bing, D.-D. Yang, Y. Yang, G.-H. Liao, L.-J. Wang, Crystengcomm, 13 (2011) 4486-4490.
[130] W. Wu, S.F. Zhang, F. Ren, X.H. Xiao, J. Zhou, C.Z. Jiang, Nanoscale, 3 (2011) 4676-4684.
[131] S.F. Zhang, F. Ren, W. Wu, J. Zhou, X.H. Xiao, L.L. Sun, Y. Liu, C.Z. Jiang, PCCP 15 (2013) 8228-8236.
[132] X. Zhang, H. Ren, T. Wang, L. Zhang, L. Li, C. Wang, Z. Su, J. Mater. Chem. , 22 (2012) 13380-13385.
[133] A. Hernandez, L. Maya, E. Sanchez-Mora, E.M. Sanchez, J. Sol-Gel Sci. Technol. , 42 (2007) 71-78.
[134] W. Chiu, P. Khiew, M. Cloke, D. Isa, H. Lim, T. Tan, N. Huang, S. Radiman, R. Abd-Shukor, M.A.A. Hamid, J. Phys. Chem. C, 114 (2010) 8212-8218.
[135] J.H. Sui, J. Li, Z.G. Li, W. Cai, Mater. Chem. Phys. , 134 (2012) 229-234.
[136] Y. Liu, L. Yu, Y. Hu, C.F. Guo, F.M. Zhang, X.W. Lou, Nanoscale, 4 (2012) 183-187.
[137] W. Wu, S.F. Zhang, X.H. Xiao, J. Zhou, F. Ren, L.L. Sun, C.Z. Jiang, ACS Appl. Mater. Interfaces 4(2012) 3602-3609.
[138] D. Bi, Y. Xu, Langmuir, 27 (2011) 9359-9366.
[139] H. Tong, S. Ouyang, Y. Bi, N. Umezawa, M. Oshikiri, J. Ye, Adv. Mater. , 24 (2012) 229-251.
[140] G. Xi, B. Yue, J. Cao, J. Ye, Chem-Eur J, 17 (2011) 5145-5154.
[141] S.-K. Li, F.-Z. Huang, Y. Wang, Y.-H. Shen, L.-G. Qiu, A.-J. Xie, S.-J. Xu, J. Mater. Chem. , 21 (2011) 7459-7466.
[142] Y. Wang, S. Li, X. Xing, F. Huang, Y. Shen, A. Xie, X. Wang, J. Zhang, Chem-Eur J, 17 (2011) 4802-4808.
[143] C. Zou, Y. Rao, A. Alyamani, W. Chu, M. Chen, D.A. Patterson, E.A. Emanuelsson, W. Gao, Langmuir, 26 (2010) 11615-11620.
[144] A.G. Prado, L.B. Bolzon, C.P. Pedroso, A.O. Moura, L.L. Costa, Appl. Catal. B, 82 (2008) 219-224.
[145] S. Ge, H. Jia, H. Zhao, Z. Zheng, L. Zhang, J. Mater. Chem. , 20 (2010) 3052-3058.
[146] T. Murase, H. Irie, K. Hashimoto, J. Phys. Chem. B, 108 (2004) 15803-15807.
[147] S.-T. Bae, H. Shin, S. Lee, D.W. Kim, H.S. Jung, K.S. Hong, Reaction Kinetics, Mechanisms and Catalysis, 106 (2012) 67-81.
[148] L. Xu, J. Wang, Environmental Science & Technology, 46 (2012) 10145-10153.
[149] N. Wetchakun, S. Chaiwichain, B. Inceesungvorn, K. Pingmuang, S. Phanichphant, A.I. Minett, J. Chen, ACS Appl. Mater. Interfaces 4(2012) 3718-3723.
[150] H. Yang, R. Shi, J. Yu, R. Liu, R. Zhang, H. Zhao, L. Zhang, H. Zheng, J. Phys. Chem. C, 113 (2009) 21548-21554.
[151] A. Di Paola, E. García-López, G. Marcì, L. Palmisano, J. Hazard. Mater. , 211 (2012) 3-29.
[152] Y. Lei, S. Song, W. Fan, Y. Xing, H. Zhang, J. Phys. Chem. C, 113 (2009) 1280-1285.
[153] Y. Hu, Y. Liu, H. Qian, Z. Li, J. Chen, Langmuir, 26 (2010) 18570–18575.
[154] T. Wu, X. Zhou, H. Zhang, X. Zhong, Nano Res, 3 (2010) 379-386.
[155] Y.C. Zhang, J. Li, M. Zhang, D.D. Dionysiou, Environmental science & technology, 45 (2011) 9324-9331.
[156] F. Cao, W. Shi, L. Zhao, S. Song, J. Yang, Y. Lei, H. Zhang, J. Phys. Chem. C, 112 (2008) 17095-17101.
[157] X. Liu, Z. Fang, X. Zhang, W. Zhang, X. Wei, B. Geng, Cryst. Growth Des., 9 (2008) 197-202.
[158] Y. Shi, H. Li, L. Wang, W. Shen, H. Chen, ACS Appl. Mater. Interfaces 4(2012) 4800-4806.
[159] S. Luo, F. Chai, L. Zhang, C. Wang, L. Li, X. Liu, Z. Su, J. Mater. Chem. , 22 (2012)

4832-4836.
[160] W. Li, D. Li, W. Zhang, Y. Hu, Y. He, X. Fu, J. Phys. Chem. C, 114 (2010) 2154-2159.
[161] X. Xu, R. Lu, X. Zhao, S. Xu, X. Lei, F. Zhang, D.G. Evans, Appl. Catal. B, 102 (2011) 147-156.
[162] J. Shi, H.n. Cui, Z. Liang, X. Lu, Y. Tong, C. Su, H. Liu, Energy Environ. Sci. , 4 (2011) 466-470.
[163] W. Zhang, X. Zhong, Inorg. Chem. , 50 (2011) 4065-4072.
[164] Z. Chen, D. Li, W. Zhang, Y. Shao, T. Chen, M. Sun, X. Fu, J. Phys. Chem. C, 113 (2009) 4433-4440.
[165] Y. Chen, S. Hu, W. Liu, X. Chen, L. Wu, X. Wang, P. Liu, Z. Li, Dalton Trans. , 40 (2011) 2607-2613.
[166] H. Yu, X. Quan, Prog Chem, 21 (2009) 406-419.
[167] Z. Zhang, J.T. Yates, Chem. Rev. , 112 (2012) 5520-5551.
[168] W.Y. Teoh, J.A. Scott, R. Amal, J. Phys. Chem. Lett., 3 (2012) 629-639.
[169] Y. Shaogui, Q. Xie, L. Xinyong, L. Yazi, C. Shuo, C. Guohua, PCCP 6(2004) 659-664.
[170] Y. Liao, H. Li, Y. Liu, Z. Zou, D. Zeng, C. Xie, J. Comb. Chem. , 12 (2010) 883-889.
[171] H.-i. Kim, J. Kim, W. Kim, W. Choi, J. Phys. Chem. C, 115 (2011) 9797-9805.
[172] J.S. Chen, C. Chen, J. Liu, R. Xu, S.Z. Qiao, X.W. Lou, Chem. Commun. , 47 (2011) 2631-2633.
[173] X.-L. Dong, X.-Y. Mou, H.-C. Ma, X.-X. Zhang, X.-F. Zhang, W.-J. Sun, C. Ma, M. Xue, J. Sol-Gel Sci. Technol. , 66 (2013) 231-237.
[174] Y. Zhang, X. Yu, Y. Jia, Z. Jin, J. Liu, X. Huang, Eur. J. Inorg. Chem. , 2011 (2011) 5096-5104.
[175] E. Stratakis, E. Kymakis, Mater. Today 16 (2013) 133-146.
[176] L.L. Sun, W. Wu, S.L. Yang, J. Zhou, M.Q. Hong, X.H. Xiao, F. Ren, C.Z. Jiang, ACS Appl. Mater. Interfaces 6(2014) 1113-1124.
[177] Y. Lin, Z. Geng, H. Cai, L. Ma, J. Chen, J. Zeng, N. Pan, X. Wang, Eur. J. Inorg. Chem. , 2012 (2012) 4439-4444.
[178] Y.C. Tang, C. HU, Y.Z. Wang, H.P. Zhang, X.H. Huang, Prog Chem, 17 (2005) 225-230.
[179] Z. Chen, N. Zhang, Y.-J. Xu, Crystengcomm, 15 (2013) 3022-3030.
[180] Y. Zhang, Z. Chen, S. Liu, Y.-J. Xu, Appl. Catal. B, 140–141 (2013) 598-607.
[181] P. Sheng, W. Li, J. Cai, X. Wang, X. Tong, Q. Cai, C.A. Grimes, J Mater Chem A, 1 (2013) 7806-7815.
[182] L. Zhang, H.H. Mohamed, R. Dillert, D. Bahnemann, "J. Photochem. Photobiol., C ", 13 (2012) 263-276.
[183] Y. Gao, Materials Science and Engineering: R: Reports, 68 (2010) 39-87.
[184] M.M. Waegele, X. Chen, D.M. Herlihy, T. Cuk, J. Am. Chem. Soc. , 136 (2014) 10632-10639.
[185] V. Zhukov, V. Tyuterev, E. Chulkov, P. Echenique, Int. J. Photoenergy 2014 (2014) 738921.
[186] N.G. Petrik, G.A. Kimmel, J. Phys. Chem. Lett., 1 (2010) 1758-1762.
[187] P.S. Marcos, J. Marto, T. Trindade, J. Labrincha, "J. Photochem. Photobiol., A ", 197 (2008) 125-131.
[188] D. Tsoukleris, A. Kontos, P. Aloupogiannis, P. Falaras, Catal. Today 124 (2007) 110-117.
[189] E. Rego, J. Marto, P.S. Marcos, J. Labrincha, "Appl. Catal., A ", 355 (2009) 109-114.
[190] S. Nishimoto, A. Kubo, K. Nohara, X. Zhang, N. Taneichi, T. Okui, Z. Liu, K. Nakata, H. Sakai, T. Murakami, Appl. Surf. Sci. , 255 (2009) 6221-6225.
[191] P. Dzik, M. Vesely, J. Chomoucka, J Adv Oxid Technol, 13 (2010) 172-183.
[192] M. Arin, P. Lommens, N. Avci, S.C. Hopkins, K. De Buysser, I.M. Arabatzis, I. Fasaki, D. Poelman, I. Van Driessche, J. Eur. Ceram. Soc. , 31 (2011) 1067-1074.

[193] M. Morozova, P. Kluson, J. Krysa, P. Dzik, M. Vesely, O. Solcova, Sens. Actuators B, 160 (2011) 371-378.
[194] T. Kawahara, K. Doushita, H. Tada, J. Sol-Gel Sci. Technol. , 27 (2003) 301-307.
[195] K. Nakata, A. Fujishima, "J. Photochem. Photobiol., C ", 13 (2012) 169-189.
[196] R.M. Pasquarelli, D.S. Ginley, R. O'Hayre, Chem. Soc. Rev. , 40 (2011) 5406-5441.
[197] Y. Xia, L. Yin, PCCP 15 (2013) 18627-18634.
[198] Q. Tian, W. Wu, L. Sun, S. Yang, M. Lei, J. Zhou, Y. Liu, X. Xiao, F. Ren, C. Jiang, V.A.L. Roy, ACS Appl. Mater. Interfaces 6(2014) 13088-13097.

Figure Captions

Figure 1 Schematic presentation of the typical hysteresis loops of magnetic iron oxide nanoparticles.

Figure 2 Band gap energy, VB and CB for a range of semiconductors on a potential scale (V) versus the normal hydrogen electrode (NHE).

Figure 3 Typical structure types of magnetic iron oxide-semiconductors composite nanomaterials. Blue spheres represent magnetic iron oxide nanoparticles, and the non-magnetic entities and matrix materials are displayed in other colour.

Figure 4 Traditional charge transfer between two semiconductors with a narrow and wide band gap, depicting the isolation of reaction sites for oxidation and reduction in coupled semiconductor system (a); charge transfer in capped semiconductor system (b).

Figure 5 Schematic diagram showing the photogenerated charge transfer of (a) iron oxide/SiO_2/semiconductors, (b) iron oxide /semiconductors and (c) iron oxide/C/semiconductors heterojunctions.

Figure 6 Scheme of the preparation of iron oxides-semiconductors composite nanomaterials by seed-mediated growth method.

Figure 7 Scheme of the preparation of iron oxides-semiconductors composite nanomaterials by layer-by-layer deposition method.

Figure 8 Scheme depicting α-Fe_2O_3/TiO_2 (TiO_2 grains in spindle-like α-Fe_2O_3) bi-component NPs synthesis by ion implantation method. [113]

Figure 9 Scheme of the reuse of cyclodextrin-functionalized Fe_3O_4@TiO_2 for photocatalytic degradation of endocrine-disrupting chemicals in water supplies. [121]

Figure 10 Schematically illustrated formation process of hierarchically assembled SnO_2/α-Fe_2O_3

heterostructures based on α-Fe_2O_3 nanospindle precursor. [127]

Figure 11 TEM image (a) and photograph of magnetic separation of spindle-like iron oxide/SnO_2 composite nanoparticles. [130]

Figure 12 Synthetic route and formation mechanism for fabricating the mesoporous hematite-ZnO core-shell composite particles. [137]

Figure 13 Formation of the Fe_3O_4/WO_3 core-shell structures: a) polycrystalline Fe_3O_4 microspheres; b) Fe_3O_4 microspheres coated with a thin layer of $W_{18}O_{49}$; c) $Fe_3O_4/W_{18}O_{49}$ core–shell structures; d) Fe_3O_4/WO_3core-shell structures obtained by oxidizing $Fe_3O_4/W_{18}O_{49}$ in air. [140]

Figure 14 SEM image and photocatalytic performances of α-Fe_2O_3/CdS corn-like nanorods under visible light irradiation. [158]

Figure 15 Scheme of the preparation of iron oxides-multiple semiconductor layers composite photocatalysts.

Figure 16 Synthetic route (a) and SEM, and TEM images for fabricating the ellipsoidal α-$Fe_2O_3/SiO_2/SnO_2/TiO_2$ composite photocatalytic nanomaterials (b). [172]

Figure 17 Depiction of various semiconductor solution deposition methods by printing. [196]

Figures

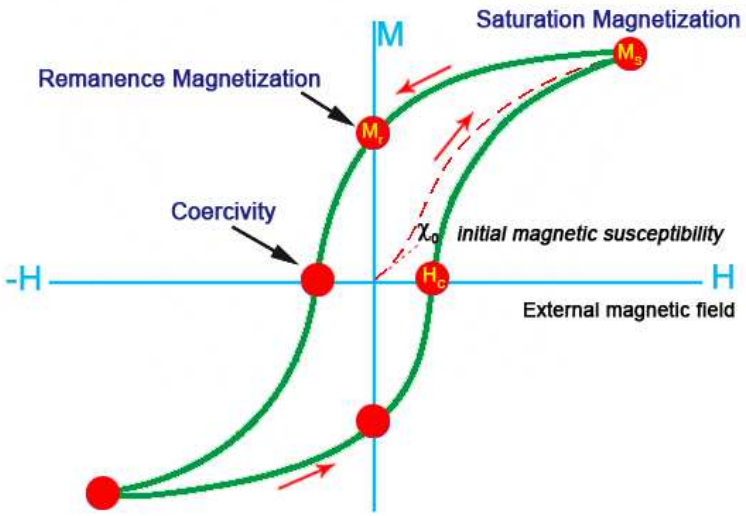

Figure 1

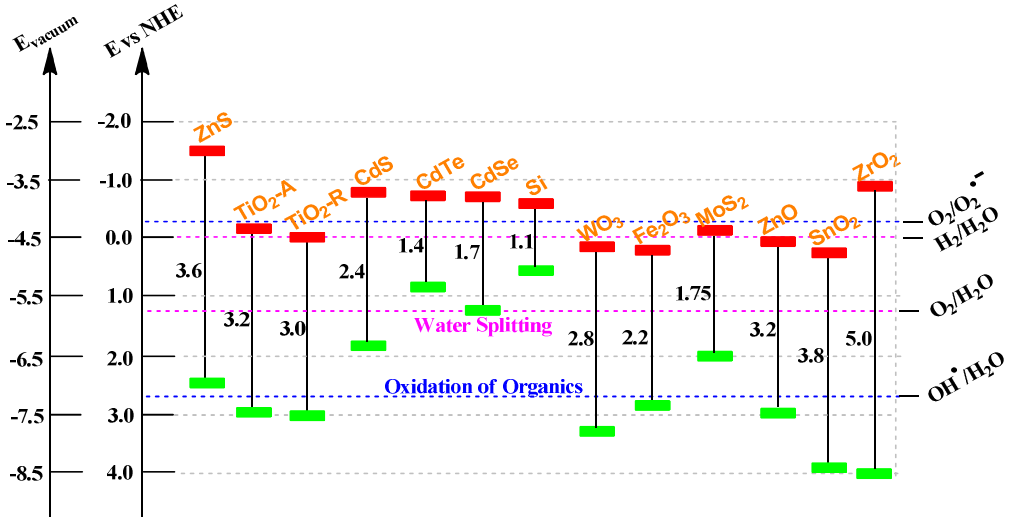

Figure 2

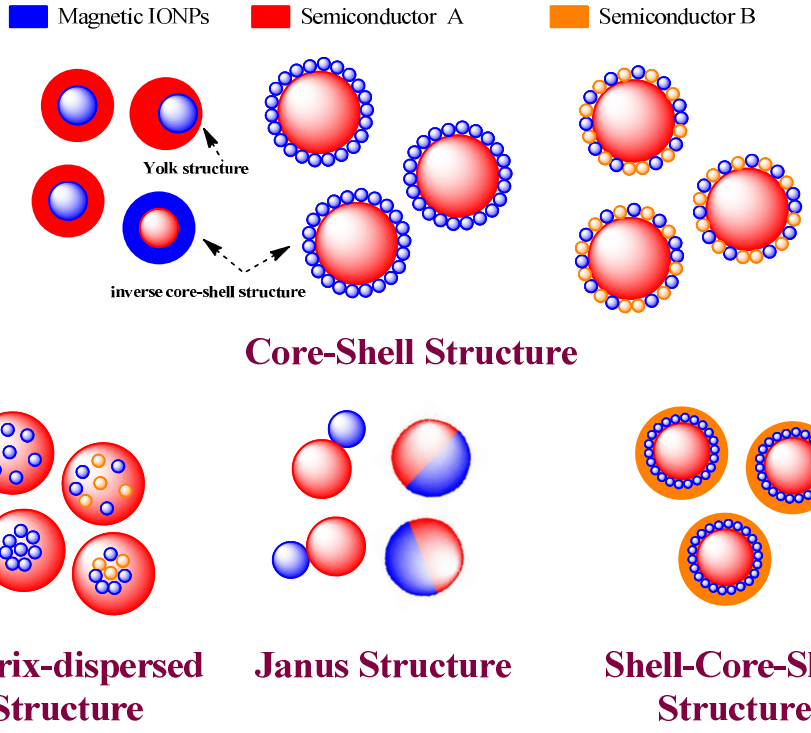

Figure 3

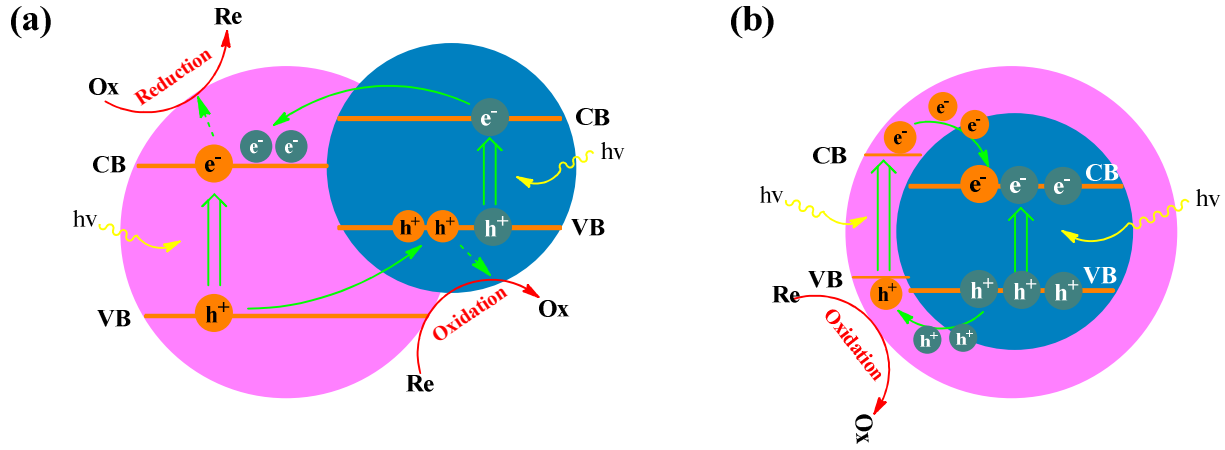

Figure 4

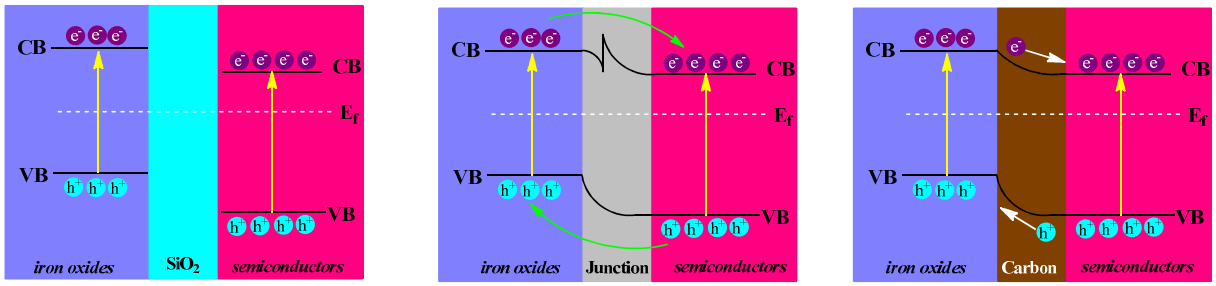

(a) A Insulated Layer (b) Direct Contact (c) A Conductive Layer

Figure 5

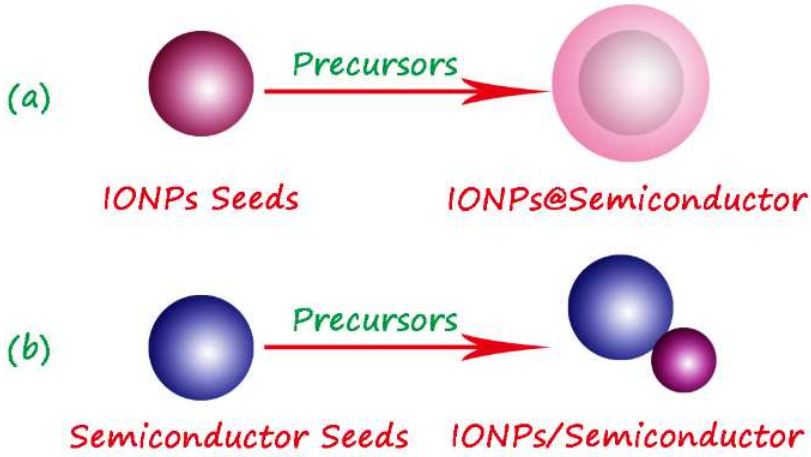

Figure 6

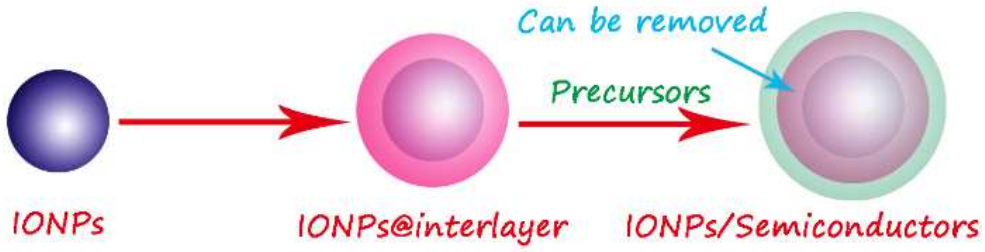

Figure 7

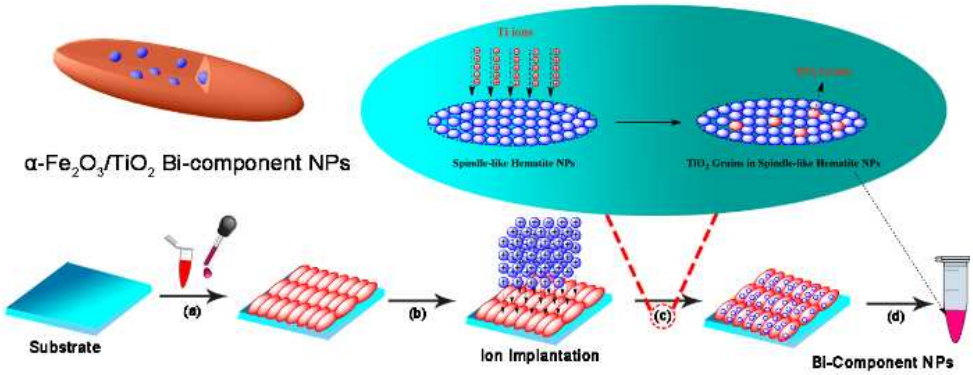

Figure 8

Figure 9

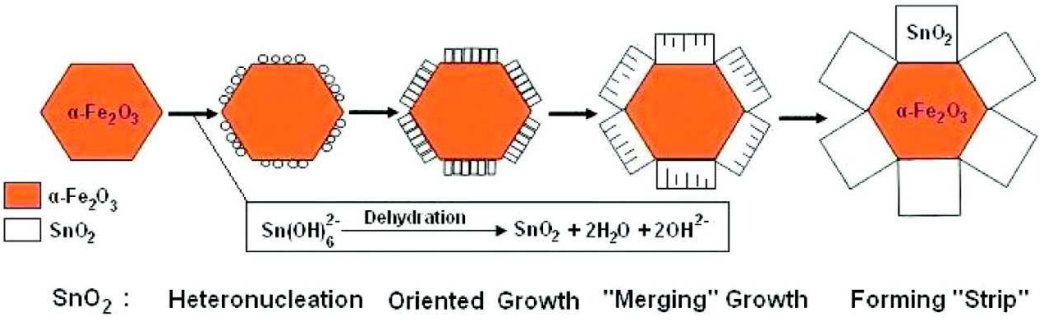

Figure 10

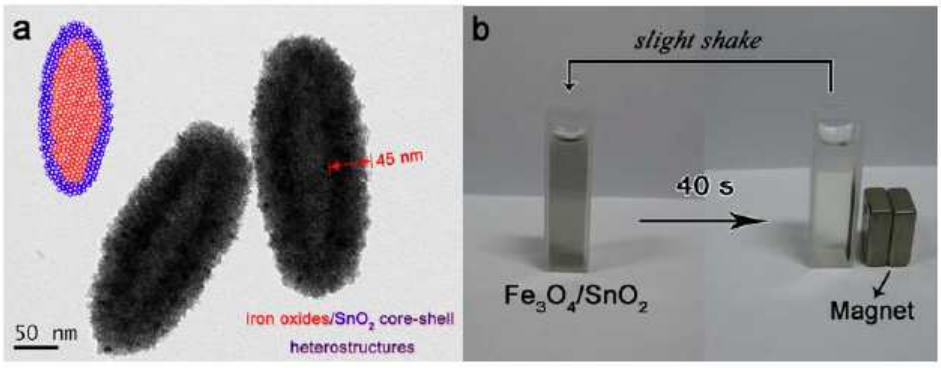

Figure 11

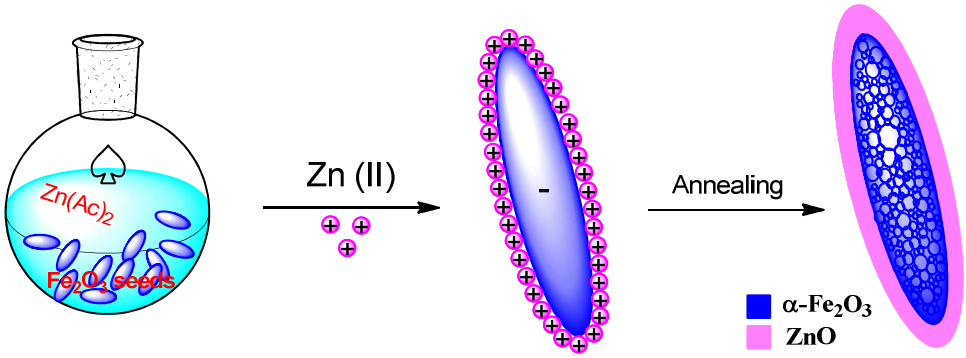

Figure 12

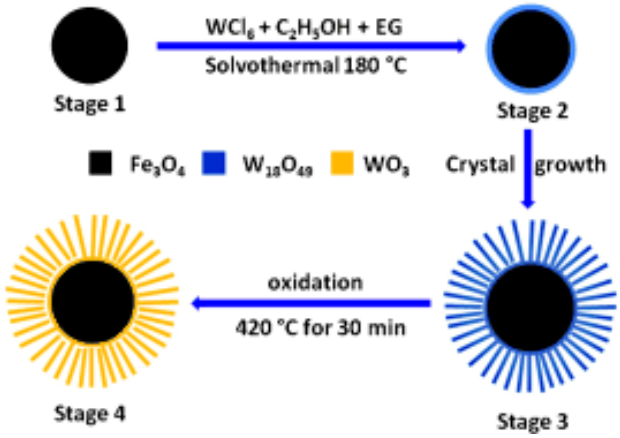

Figure 13

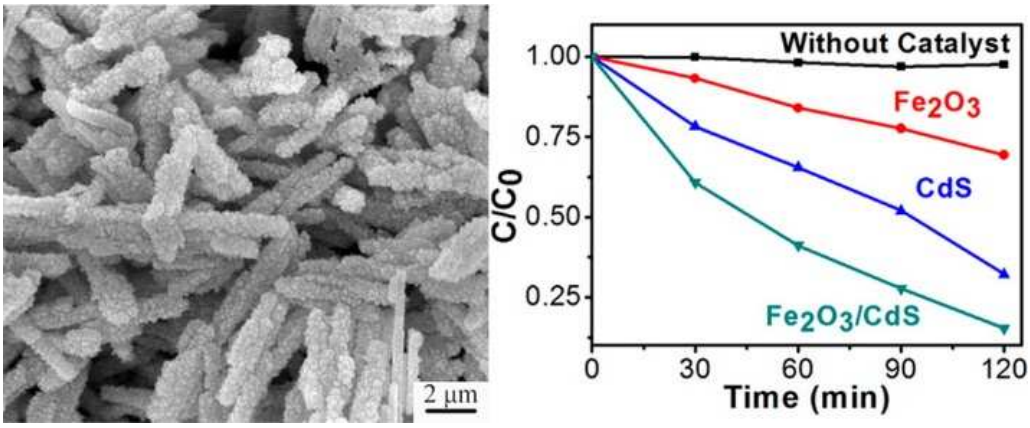

Figure 14

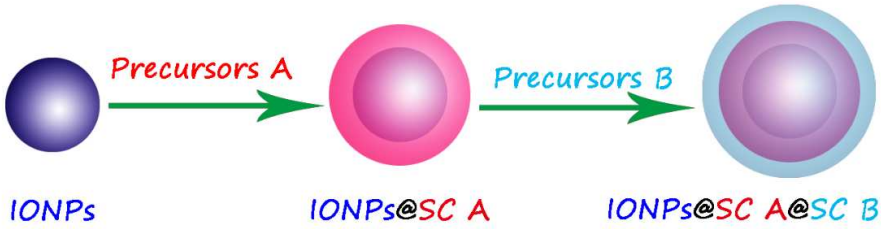

SC: Semiconductor

Figure 15

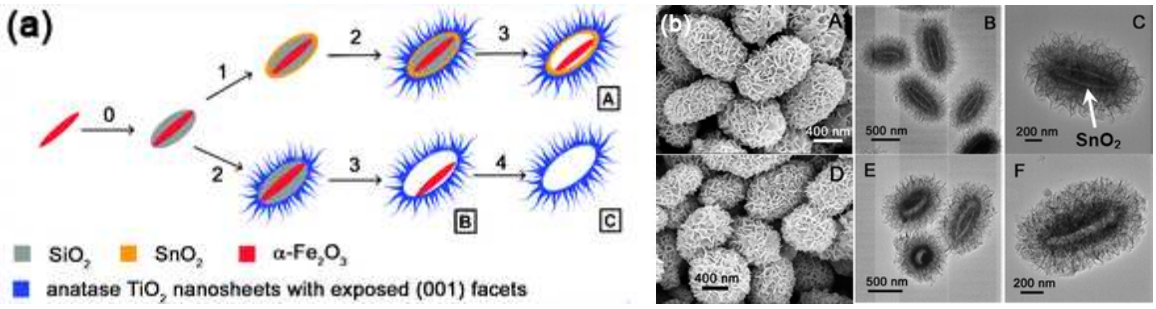

Figure 16

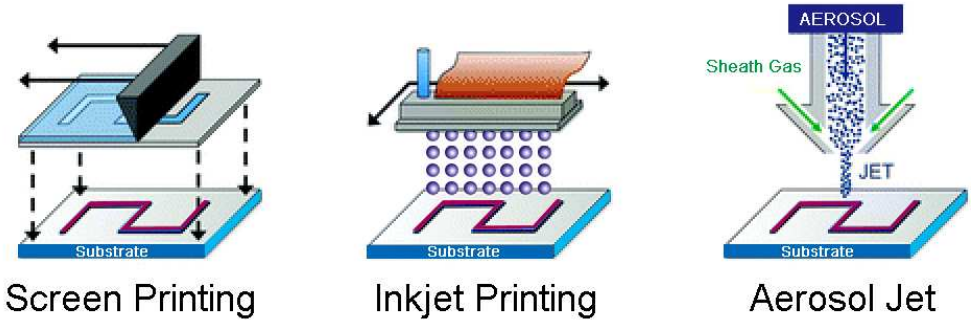

Figure 17

Table 1 The representative magnetic iron oxide-semiconductor photocatalysts and their photocatalytic perfermance

Structure	Materials	Pollutants	Light Resource	Rate Constant *k* (10^{-2} min^{-1})	Stability Perfermance	Ref.
Binary structure	Fe_3O_4@TiO_2	Bisphenol A	UV light	-[a]	90% after 10 cycles	[121]
	α-Fe_2O_3@ TiO_2	RhB	Visible-light	0.81	-	[197]
	γ-Fe_2O_3@SnO_2	RhB	UV light	0.68	-	[131]
	α-Fe_2O_3@ZnO	RhB	UV+visible light	2.4	-	[137]
	Fe_3O_4@WO_3	MB	Visible-light	-b	no obvious decrease after 3 cycles	[140]
	Fe_3O_4/ZnS	Eosin Y	UV light	-[c]	95% after 15 cycles	[112]
	α-Fe_2O_3/CdS	MB	Visible-light	1.68	-	[158]
Ternary struture	Fe_3O_4@SiO_2@TiO_2	Methyl orange	UV light	-	91% after 6 cycles	.[120]
	Graphene-TiO_2-Fe_3O_4	RhB	UV light	16	no obvious decrease after 5 cycles	[177]
	α-Fe_2O_3@SnO_2@Cu_2O	RhB	UV+visible light	3.29	85% after 8 cycles	[198]
Multiple layers structure	α-Fe_2O_3/Ag/SiO_2/SnO_2	RhB	UV light	0.13	-	[176]
			Visible ligth	0.41	-	
			UV+visible light	7.21	96% after 8 cycles	
	α-Fe_2O_3/SiO_2/SnO_2/TiO_2	MB	UV light	0.29[d]	-	[172]

Note: a, photocatalytic degradation of BPA is complete within 60 min; b, photocatalytic degradation of MB is complete within 120 min; c, photocatalytic degradation of Eosin Y is complete within 37 min; d, photocatalytic degradation of MB is 70% within 120 min.